Advances in Nano Research, *Vol. 10, No. 1 (2021) 25-42*
DOI: https://doi.org/10.12989/anr.2021.10.1.025

Size dependent vibration of embedded functionally graded nanoplate in hygrothermal environment by Rayleigh-Ritz method

Piyush P. Singh[a] and Mohammad S. Azam[*]

Department of Mechanical Engineering, Indian Institute of Technology (Indian School of Mines), Dhanbad, Jharkhand, India

(*Received June 29, 2020, Revised September 26, 2020, Accepted September 29, 2020*)

Abstract. In this article, the vibration behavior of embedded Functionally Graded Nanoplate (FGNP) employing nonlocal Kirchhoff's plate theory has been investigated under hygrothermal environment. The FGNP is considered to be supported by Winkler-Pasternak foundation. The Eringen's differential theory is used for size effect on the vibration of the FGNP. Rayleigh-Ritz method with orthogonal polynomials are employed for the governing equations and edge constraints. The advantage of this method is that it overcomes all the drawbacks of edge constraints and can easily handle any combinations of mixed edge constraints. The coefficients viz. moisture expansion, thermal expansion and elastic coefficients are considered to be transversely graded across the FGNP. The similarity of the calculated natural frequencies is examined with the previous research, and a good concurrency is seen. The objective of this article is to analyze the parameters' effect on the nondimensionalized frequency of embedded FGNP under hygrothermal environment subjected to all possible edge constraints. For this, uniform and linear rise of temperature and moisture concentration are considered. The study highlights that the nonlocal effect is pronounced for higher modes. Moreover, the effect of the Pasternak modulus is seen to be prominent compared to the Winkler modulus on non dimensionalized frequencies of FGNP.

Keywords: functionally graded plate; nanoplate; vibration analysis; Winkler-Pasternak foundation; hygrothermal environment; Rayleigh-Ritz

1. Introduction

With the increase in complexity of use, the laminated composite material has failed to serve the purpose. In laminated composites, delamination occurs, which reduces the stiffness leading to the failure of the structure. To overcome the drawback, Functionally Graded Materials (FGMs) were introduced in 1872. FGMs are made up of two or more constituent having continuous and smoothly varying composition in a particular direction. In commonly used FGMs, the ceramic part acts as thermal blockade and the metallic part provides better fracture resistance (Ehyaei *et al*. 2016). These materials are superior to other composites made up of the same constituents. FGMs have many advantages, which includes reduction in stresses, better thermal resistivity and high toughness. Due to the enhanced properties, FGM structures are being used in various engineering fields such as aerospace, electronics, mechanical, biomedical, nuclear, etc., for last few decades. Motivated by wide range of applications, different researchers (Zine *et al*. 2020, Khiloun *et al*. 2020, Rahmani *et al*. 2020, Matouk *et al*. 2020, Hussain *et al*. 2020a, Al-Furjan *et al*. 2020, Boussoula *et al*. 2020, Bousahla *et al*. 2020) have analyzed the bending, buckling and vibration to ensure the safe design of the FGM structures.

Power law and exponential law are two commonly employed properties variation rules to examine the properties of FGM (Ebrahimi and Barati 2017). Nanoplates made of FGMs are an important component of nanodevices. For an accurate design of these devices, vibration analysis is one of the important aspects (Hołubowski *et al*. 2019). As at nanoscale, an experiment is expensive to perform; hence an efficient mathematical method is needed to analyze the vibration of FGNP. The interatomic forces amend the dynamic behavior of nanoplates as these forces become significant at small scales. If these effects are neglected, it may cause inaccuracy in the solution, leading to erroneous design.

With regard to the nanoplate, atomistic, hybrid atomistic-continuum mechanics and continuum mechanics are the three proposed methods that are used. The atomistic approach can only be used for systems with fewer atoms and molecules. This method is computationally expensive and cannot handle a large number of equations (Malekzadeh and Shojaee 2015). Classical continuum models do not consider the surface effect as it is the scale-free model (Barati 2017). Some theories, however, consider the scale effect but are complex to use; hence Eringen's theory is commonly used. This theory considers scale effect in predicting the behavior of nanoplates accurately with less computational effort (Eringen 1972, 2002), according to which, at a point, stress is the function of a strain and the spatial integral of the average of strains of neighboring points. In the case of the classical model, the stresses depend on the strains at a specified point (Barati 2018).

*Corresponding author, Ph.D., Professor,
E-mail: mdsazam@iitism.ac.in; mdsazam@gmail.com
[a] Ph.D. Student

Copyright © 2021 Techno-Press, Ltd.

ISSN: 2287-237X (Print), 2287-2388 (Online)

With the unique characteristics, FGM nanostructures have become an ideal candidate for the multifarious field of nanotechnology. Recently, various researchers (Ehyaei and Daman 2017, Bensaid *et al*. 2018, Bouadi *et al*. 2018, Bedia *et al*. 2019, Hussain *et al*. 2019, 2020b, Taj *et al*. 2020, Matouk *et al*. 2020, Boutaleb *et al*. 2019, Balubaid *et al*. 2019) have studied bending, buckling and dynamic behavior of nanostructures using Eringen's theory.

In many applications, FGNP embedded in an elastic medium is widely used. To analyze interaction, many models are proposed. According to the Winkler model (Winkler 1867), a series of discrete, closely spaced linear homogeneous springs are used as the foundation. One of the major limitations of this model is deformation is restrained to the loaded region only. Further, the major problem with this model is to find the spring stiffness. Various studies were published in which attempts were made by researchers (Hetenyi 1950, Filonenko-Borodich 1940) to solve the problems linked with the Winker model. The two-parameter elastic medium model was proposed according to which a shear interaction between the adjacent points in the foundation was considered. But the fundamental problem linked with these models was the shear parameter used in these models, which can only be experimentally determined. Proposed in 1954, the Pasternak model (Pasternak 1954), a two-parameter elastic model, is employed for a practical depiction of the elastic medium. Moreover, the shear factor in Pasternak's elastic medium model need not be determined experimentally, and it is an accurate model. According to this model, a shear interaction layer amidst the Winkler's springs is assumed by connecting the end of springs to a shear layer. The two parameters in Pasternak's elastic substrate model respectively show the normal pressure and the transverse shear stress due to the shear deformation of the foundation. Further, this model was referred to as the generalized foundation model. Recently, several works have been carried out (Bourada *et al*. 2020, Chikr *et al*. 2020, Kaddari *et al*. 2020, Shariati *et al*. 2020, Addou *et al*. 2019, Tounsi *et al*. 2020, Semmah *et al*. 2019) to analyze the structural behavior of beams and plates resting on the elastic foundation.

Composite structures in the thermal environment have attracted many researchers due to their applicability under such conditions. Many researchers have studied the behavior of different structures (plate, beam and shell) under thermal conditions. Daikh *et al*. (2020a), Matouk *et al*. (2020) and Bensaid *et al*. (2020) analyzed the vibration and buckling behavior of FG nanobeam under thermal condition. Analysis of the FG shell in the thermal environment was carried out by Daikh (2020). Further, Daikh *et al*. (2020b) analyzed the simply supported FG nanoplate resting on Kerr foundation using Hamilton's principle. Daikh (2019) gave an exact solution for nonlinear temperature distribution for the vibration of simply supported FG plate supported by elastic foundation (Winkler/Pasternak/Kerr foundation) using TSDT and Hamilton's principle. Singh and Harsha (2020) using Galerkin Vlasov's method obtained the bending and stress solution of porous sandwich SFG plate. Daikh and Megueni (2020) studied the thermal buckling of simply supported FG sandwich plate having a homogeneous face sheet using HSDT. Singh and Harsha (2019) derived the governing equations using Galerkin approach in conjunction with stress function method for the nonlinear vibration analysis. The most of the studies discussed above are related to the analysis of plate in a thermal environment, and very few pieces of literature are available dealing with the analysis of the nanoplate under hygrothermal condition.

Numerous researchers (Aksencer and Aydogdu 2011, Bendaho *et al*. 2019, Belkorissat *et al*. 2015, Chen *et al*. 2009, Bellal *et al*. 2020, Asghar *et al*. 2020) have employed various techniques to study the vibration behavior of nanoplate. Analooei *et al*. (2013) analyzed the vibration and buckling behavior of orthotropic nanoplate employing sFSM. However, in sFSM different shape functions need to be assumed to define the longitudinal and transverse deflection. Moreover, sFSM can be used for a structure having simple edge conditions only. Employing MSGT in conjugation with GDQM, Dehshahri *et al*. (2020) analyzed the natural frequency of 3 dimensional FGM nanoplate. Using FEM, analysis of vibration of CNT-FGNP was carried out by George *et al*. (2018). This method can be used to find deflection at any point, but the mechanics of the element remain unknown and many elements are required, which needs more time and effort. Karličić *et al*. (2014) used Navier solution and trigonometric method for the vibration problem of embedded nanoplates. However, the Navier solution can be used only for specified BC and cannot be generalized and the extent of the trigonometric method is that it needs a high number of terms requiring considerable iterations. Lei *et al*. (2016) studied the stability and dynamic characteristics of CNT-reinforced FG plate employing the kp-Ritz method. In this method, 2-D kernel particles' deflection factor shape function is cumbersome to find. Behrouz and Sara (2019) analyzed the FG nanoplate in a thermal environment employing unknown refined plate theory and the Galerkin method. Dynamic analysis of FGNP using 3D HSDT and nonlocal theory was conducted by Boutaleb *et al*. (2019). Vibration analysis of cracked CNT in the thermal environment using Eringen in the framework of Euler-Bernoulli theory was performed by Ebrahimi and Mahmoodi (2018). Daikh *et al*. (2020c), using Navier's solution, analyzed the free vibration behavior of FG sandwich nanoplate in thermal environment. Ebrahimi and Heidari (2018) studied the vibration characteristic of nanoplate in a humid thermal environment employing Reddy's theory with DQ method.

The limitations of the discussed methodologies in terms of efficiency of the method, accuracy of use, handling BCs can be overcome by the use of the methodology proposed in this paper. Nonlocal Kirchhoff's plate theory with the Rayleigh-Ritz method is adopted for deriving the mathematical model to study the vibration of embedded FGNP in the hygrothermal environment. The characteristics polynomials used in maximum transverse deflection expression, can handle any possible combination of BCs efficiently. As per the authors' knowledge, the effect of hygral and thermal environment on FGNP supported by Winkler Pasternak foundation has been studied for the first

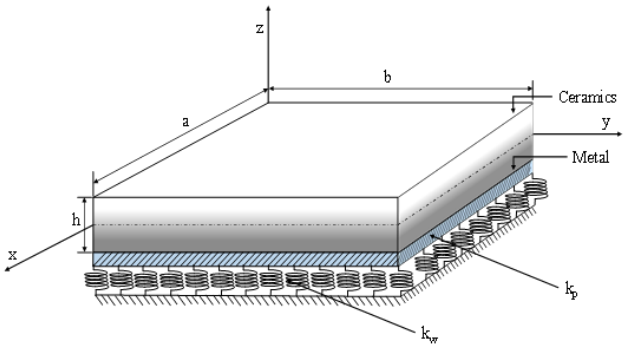

Fig. 1 Schematics of embedded functionally graded rectangular plate

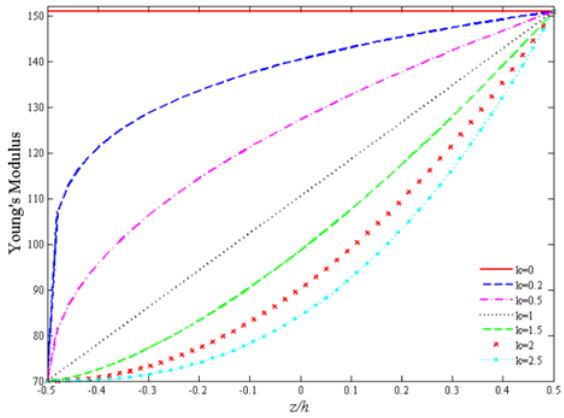

Fig. 2 Young's modulus of FGM nanoplate for different material property index

time. Further, the detailed study depicting different parameters' effect on nondimensionalized frequency (Ω) of embedded FGNP subjected to all possible combinations of the boundary constraints in the presence and the absence of the hygrothermal environment, have been conducted. The set of new results are presented for two pair of materials (Al/ZrO_2 FGM and Si_3N_4/SUS304 FGM) of FGNP in this article. The computed results by the proposed method may serve as a benchmark and may certainly be used by design engineers and practitioners for accurate design of functionally graded nanoplates in the presence as well as in the absence of the hygrothermal environment.

2. Geometry and material properties

FG plate presented in Fig. 1 has been used for the study. For the purpose of mathematical modeling, the edges of embedded FGNP are considered along the axes, *x*, *y* and *z*. The middle surface is taken at $z = 0$ and the origin is considered at the corner of the mid plane of FGNP.

The FGNP is having continuously changing material properties along thickness ($E(z)$ and $\rho(z)$) direction following power-law as (Berghouti *et al*. 2019)

$$E(z) = (E_{ceramics} - E_{metal})V(z) + E_{metal}$$
$$\rho(z) = (\rho_{ceramics} - \rho_{metal})V(z) + \rho_{metal} \quad (1)$$

Table 1 Material properties of functionally graded nanoplate

Properties	Aluminium (metal)	Zirconia (ceramic)
E	70 GPa	151 GPa
v	0.3	0.3
ρ	2700 kg/m^3	3000 kg/m^3

Here

$$V(z) = \left(\frac{2z+h}{2h}\right)^k \quad (2)$$

where $V(z)$, h and k ($k \geq 0$) are volume fraction, thickness and property exponent, respectively.

It is mathematically proven that the Poisson's ratio (υ) effect is negligible (Delale and Erdogan 1983), hence constant υ is assumed. The properties of FGNP gradually changes from ceramic to a metallic when k shifts from 0 to infinite (Fig. 2).

The contributing materials of the FGNP are reported in Table 1.

3. Mathematical modeling

3.1 Kinematics

The kinematic variables of FGNP follow CPT. Accordingly, the displacements of an imaginary point on the plate is

$$u = \begin{Bmatrix} v_x(x,y,t) \\ v_y(x,y,t) \\ v_z(x,y,t) \end{Bmatrix} = \begin{Bmatrix} -z\dfrac{\partial w(x,y,t)}{\partial x} \\ -z\dfrac{\partial w(x,y,t)}{\partial y} \\ w(x,y,t) \end{Bmatrix} \quad (3)$$

where v_x, v_y, v_z and w are components of displacement and deflection of an arbitrary point on the mid plane. The linear strain is

$$\begin{Bmatrix} \varepsilon_x \\ \varepsilon_y \\ \gamma_{xy} \end{Bmatrix} = \begin{Bmatrix} \dfrac{\partial v_x}{\partial x} \\ \dfrac{\partial v_y}{\partial y} \\ \dfrac{\partial v_x}{\partial y} + \dfrac{\partial v_y}{\partial x} \end{Bmatrix} = \begin{Bmatrix} -z\dfrac{\partial w}{\partial x^2} \\ -z\dfrac{\partial w}{\partial y^2} \\ -2z\dfrac{\partial^2 w}{\partial x \partial y} \end{Bmatrix} \quad (4)$$

where normal strains and shear strain are denoted by, ε_x, ε_y and γ_{xy} respectively.

3.1 Nonlocal elasticity

Using Eringen's theory, the nonlocal stress tensor is given as (Ebrahimi and Shafiei 2017)

$$\sigma^{nl} = \int_v K(|x' - x|, \tau)\, \sigma^l(x')dx \quad (5)$$

where $\sigma^l(x')$ is the local stress tensor at point x, $K(|x'-x|,\tau)$ is nonlocal modulus and $|x'-x|$ represents the lattice parameters. The relation of the nonlocal stress and strain of the Hookean solid is given by

$$(1-\tau^2c^2\nabla^2)\sigma^{nl}=S:\varepsilon \tag{6}$$

$$\tau=\frac{e_0 l}{c} \tag{7}$$

$$(1-(e_0 l)^2\nabla^2)\sigma^{nl}=S:\varepsilon \tag{8}$$

$$\mu=(e_0 l)^2 \tag{9}$$

Here, ∇^2 is Laplacian operator as $\nabla^2=\frac{\partial^2(\blacksquare)}{\partial x^2}+\frac{\partial^2(\blacksquare)}{\partial y^2}$, σ^{nl} is nonlocal stress tensor, ":" is the double dot product, S is an elasticity tensor of 4th order and ε is strain tensor. The term μ is known as nonlocal parameter which helps to include the scale effect expressed in terms of the characteristic internal length, e_0 is the constant predicted experimentally, l is characteristic internal length, and c is characteristic external length. The value of the nonlocal parameter is related to the chirality, the mode shapes, and the nature of motions (Hosseini-Hashemi *et al*. 2013). This parameter cannot be calculated accurately; however, it is considered that this parameter can be obtained by the comparison of dispersion curves from nonlocal elasticity and lattice dynamics of nanomaterial structure (Boutaleb *et al*. 2019). On reducing μ to zero, the nonlocal effect diminishes. A conservative estimate of the scale coefficient for the case of nanoplate is in the range of $0 \le \mu \le 4$.

3.3 Consecutive relations

Using Eq. (8), the constitutive stress-strain relationship of the nanoplate is written as

$$\begin{Bmatrix}\sigma_x^{nl}\\ \sigma_y^{nl}\\ \tau_{xy}^{nl}\end{Bmatrix}-(\mu\nabla^2)\begin{Bmatrix}\sigma_x^{nl}\\ \sigma_y^{nl}\\ \tau_{xy}^{nl}\end{Bmatrix}= \begin{bmatrix}C_{11} & C_{12} & 0\\ C_{21} & C_{22} & 0\\ 0 & 0 & C_{66}\end{bmatrix}\begin{Bmatrix}\varepsilon_x\\ \varepsilon_y\\ \gamma_{xy}\end{Bmatrix} \tag{10}$$

Here, $(\sigma_x,\sigma_y,\tau_{xy})$ and $(\varepsilon_x,\varepsilon_y,\gamma_{xy})$ are stress and strain components respectively, and stiffness components for the FGNP are expressed as

$$C_{11}=C_{22}=\frac{E(z)}{1-\nu^2} \tag{11a}$$

$$C_{12}=C_{21}=\frac{\nu E(z)}{1-\nu^2} \tag{11b}$$

$$C_{66}=\frac{E(z)}{2(1+\nu)} \tag{11c}$$

According to nonlocal plate model, the actual stress tensor is σ_{ij}^{nl} and τ_{ij}^{nl} and not σ_{ij}^{l} and τ_{ij}^{l}. Further, the resultant stress (N) and moment (M) are given as

$$N=\begin{Bmatrix}N_x\\ N_y\\ N_{xy}\end{Bmatrix}=\int_{-\hbar/2}^{\hbar/2}\begin{Bmatrix}\sigma_x^{nl}\\ \sigma_y^{nl}\\ \tau_{xy}^{nl}\end{Bmatrix}dz$$
$$M=\begin{Bmatrix}M_x\\ M_y\\ M_{xy}\end{Bmatrix}=\int_{-\hbar/2}^{\hbar/2}z\begin{Bmatrix}\sigma_x^{nl}\\ \sigma_y^{nl}\\ \tau_{xy}^{nl}\end{Bmatrix}dz \tag{12}$$

Using Eqs. (4), (6), (10) and (12), the resultants of moments are expressed as

$$\begin{Bmatrix}M_x\\ M_y\\ M_{xy}\end{Bmatrix}-(\mu\nabla^2)\begin{Bmatrix}M_x\\ M_y\\ M_{xy}\end{Bmatrix}=\begin{bmatrix}D_{11} & D_{12} & 0\\ D_{21} & D_{22} & 0\\ 0 & 0 & D_{66}\end{bmatrix}\begin{Bmatrix}\frac{\partial^2 w}{\partial x^2}\\ \frac{\partial^2 w}{\partial y^2}\\ 2\frac{\partial^2 w}{\partial x\partial y}\end{Bmatrix} \tag{13}$$

where flexural rigidities are

$$(D_{11},D_{12},D_{66})=\int_{-\hbar/2}^{\hbar/2}(C_{11},C_{12},C_{66})z^2dz \tag{14}$$

3.4 Virtual work

Using the principle of virtual work, according to which virtual work of forces acting on the system in equilibrium is equal to zero $(\delta(U-T+V)=0)$ and nonlocal elasticity theory, the governing equations in the absence of temperature are derived (Anjomshoa 2013) as

$$\frac{\partial N_x}{\partial x}+\frac{\partial N_{xy}}{\partial y}=I_0\frac{\partial^2 v_x}{\partial t^2} \tag{15a}$$

$$\frac{\partial N_{xy}}{\partial x}+\frac{\partial N_y}{\partial y}=I_0\frac{\partial^2 v_y}{\partial t^2} \tag{15b}$$

$$\begin{aligned}&\frac{\partial^2 M_x}{\partial x^2}+2\frac{\partial^2 M_{xy}}{\partial x\partial y}+\frac{\partial^2 M_y}{\partial y^2}+\frac{\partial}{\partial x}\left(N_x\frac{\partial v_z}{\partial x}\right)+\frac{\partial}{\partial y}\\ &\left(N_y\frac{\partial v_z}{\partial y}\right)+\frac{\partial}{\partial x}\left(N_{xy}\frac{\partial v_z}{\partial y}\right)+\frac{\partial}{\partial y}\left(N_{yx}\frac{\partial v_z}{\partial x}\right)+q_0\\ &-k_w+k_p\left(\frac{\partial^2 v_z}{\partial x^2}+\frac{\partial^2 v_z}{\partial y^2}\right)\\ &=I_0\frac{\partial^2 v_z}{\partial t^2}-I_1\left(\frac{\partial^4 v_z}{\partial x^2\partial t^2}+\frac{\partial^4 v_z}{\partial y^2\partial t^2}\right)\end{aligned} \tag{15c}$$

Here, k_w and k_p represent the Winkler and Pasternak coefficients, respectively. I_0 and I_1 are defined as

$$I_0=\int_{-\hbar/2}^{\hbar/2}\rho dz,\qquad I_1=\int_{-\hbar/2}^{\hbar/2}\rho z^2dz \tag{16}$$

Using Eqs. (13) and (15c) and considering the displacement component as $v_z=\bar{w}(x,y)\cos\omega t$, the following equilibrium equation for the embedded FGNP is

obtained

$$D_{11}\left(\frac{\partial^4\bar{w}}{\partial x^4}+\frac{\partial^4\bar{w}}{\partial y^4}\right)+2D_{12}\frac{\partial^4\bar{w}}{\partial x^2\partial y^2}+4D_{66}\frac{\partial^4\bar{w}}{\partial x^2\partial y^2}$$
$$-(1-\mu\nabla^2)\begin{bmatrix} q_0-k_w\bar{w}+k_p\left(\frac{\partial^2\bar{w}}{\partial x^2}+\frac{\partial^2\bar{w}}{\partial y^2}\right)\\ +I_0\omega^2\bar{w}-I_1\omega^2\left(\frac{\partial^2\bar{w}}{\partial x^2}+\frac{\partial^2\bar{w}}{\partial y^2}\right)\\ +\frac{\partial}{\partial x}\left(N_x\frac{\partial\bar{w}}{\partial x}\right)+\frac{\partial}{\partial y}\left(N_y\frac{\partial\bar{w}}{\partial y}\right)\\ +\frac{\partial}{\partial x}\left(N_{xy}\frac{\partial\bar{w}}{\partial y}\right)+\frac{\partial}{\partial y}\left(N_{yx}\frac{\partial\bar{w}}{\partial x}\right)\end{bmatrix}=0 \quad (17)$$

where $\bar{w}$ and ω are maximum deflection and frequency of vibration of nanoplate, respectively.

The principle of minimum potential energy is the basis of variational formulation, which is applicable only in the case when, at a point, stress is written in terms of strain (Dym and Shames 1973). However, in nonlocal elasticity theory, the exact relation of stress and strain at a specified point cannot be calculated. Thus, in the present solution, an inverse approach is employed to attain the energy of the FGNP in a quadratic form, which is used as the base function for the Rayleigh-Ritz method. The procedure from Adali (2009) has been followed to derive the quadratic form for vibration problem of embedded FGNP. Eq. (18) is in a strong form and the solution is tough and cumbersome to get. Hence, a weak form of the system of equations is needed. Unlike the strong form, on the field variables, a weak form needs a weaker continuity. The weak form is derived from weighted residual methods, given as

$$\int_0^a\int_0^b\begin{bmatrix} D_{11}\left(\frac{\partial^4\bar{w}}{\partial x^4}+\frac{\partial^4\bar{w}}{\partial y^4}\right)+2D_{12}\frac{\partial^4\bar{w}}{\partial x^2\partial y^2}+4D_{66}\frac{\partial^4\bar{w}}{\partial x^2\partial y^2}\\ -(1-\mu\nabla^2)\begin{Bmatrix} q_0-k_w\bar{w}+k_p\left(\frac{\partial^2\bar{w}}{\partial x^2}+\frac{\partial^2\bar{w}}{\partial y^2}\right)+I_0\omega^2\bar{w}\\ -I_1\omega^2\left(\frac{\partial^2\bar{w}}{\partial x^2}+\frac{\partial^2\bar{w}}{\partial y^2}\right)\\ +\frac{\partial}{\partial x}\left(N_x\frac{\partial\bar{w}}{\partial x}\right)+\frac{\partial}{\partial y}\left(N_y\frac{\partial\bar{w}}{\partial y}\right)\\ +\frac{\partial}{\partial x}\left(N_{xy}\frac{\partial\bar{w}}{\partial y}\right)+\frac{\partial}{\partial y}\left(N_{yx}\frac{\partial\bar{w}}{\partial x}\right)\end{Bmatrix}\end{bmatrix}\vartheta dxdy \quad (18)$$
$$=0$$

Here, the weighted function is denoted by ϑ. Breaking the Eq. (18) using divergence theorem, the weak form is

$$\int_0^a\int_0^b \dot{\Pi}^{nl}(x,y)dxdy=0 \quad (19)$$

$$\dot{\Pi}^{nl}(x,y)=\dot{U}(x,y)-\dot{T}(x,y) \quad (20)$$

where

$$\dot{U}=\int_0^a\int_0^b\begin{bmatrix} D_{11}\left(\frac{\partial^2\bar{w}}{\partial x^2}\frac{\partial^2\vartheta}{\partial x^2}+\frac{\partial^2\bar{w}}{\partial y^2}\frac{\partial^2\vartheta}{\partial y^2}\right)\\ +D_{12}\left(\frac{\partial^2\bar{w}}{\partial x^2}\frac{\partial^2\vartheta}{\partial y^2}+\frac{\partial^2\bar{w}}{\partial y^2}\frac{\partial^2\vartheta}{\partial x^2}\right)+4D_{66}\left(\frac{\partial^2\bar{w}}{\partial x\partial y}\frac{\partial^2\vartheta}{\partial x\partial y}\right)\\ +k_w\left\{\bar{w}\vartheta+\mu\left(\frac{\partial\bar{w}}{\partial x}\frac{\partial\vartheta}{\partial x}+\frac{\partial\bar{w}}{\partial y}\frac{\partial\vartheta}{\partial y}\right)\right\}\\ +k_p\begin{Bmatrix}\left(\frac{\partial\bar{w}}{\partial x}\frac{\partial\vartheta}{\partial x}+\frac{\partial\bar{w}}{\partial y}\frac{\partial\vartheta}{\partial y}\right)\\ +\mu\left(\frac{\partial^2\bar{w}}{\partial x^2}\frac{\partial^2\vartheta}{\partial x^2}+\frac{\partial^2\bar{w}}{\partial y^2}\frac{\partial^2\vartheta}{\partial y^2}+2\frac{\partial^2\bar{w}}{\partial x\partial y}\frac{\partial^2\vartheta}{\partial x\partial y}\right)\end{Bmatrix}\end{bmatrix}dxdy \quad (21)$$

$$\dot{T}=\int_0^a\int_0^b\left[\omega^2\begin{Bmatrix} I_0\left(\bar{w}\vartheta+\mu\left(\frac{\partial\bar{w}}{\partial x}\frac{\partial\vartheta}{\partial x}+\frac{\partial\bar{w}}{\partial y}\frac{\partial\vartheta}{\partial y}\right)\right)\\ +I_1\begin{Bmatrix}\left(\frac{\partial\bar{w}}{\partial x}\frac{\partial\vartheta}{\partial x}+\frac{\partial\bar{w}}{\partial y}\frac{\partial\vartheta}{\partial y}\right)\\ +\mu\left(\frac{\partial^2\bar{w}}{\partial x^2}\frac{\partial^2\vartheta}{\partial x^2}\right.\\ \left.+2\frac{\partial^2\bar{w}}{\partial x\partial y}\frac{\partial^2\vartheta}{\partial x\partial y}+\frac{\partial^2\bar{w}}{\partial y^2}\frac{\partial^2\vartheta}{\partial y^2}\right)\end{Bmatrix}\end{Bmatrix}\right]dxdy \quad (22)$$

On solving Eqs. (21) and (22), the quadratic functional equations for maximum strain energy and kinetic energy are obtained and expressed as (Anjomshoa 2013)

$$U=\frac{1}{2}\int_0^a\int_0^b\begin{bmatrix} D_{11}\left(\left(\frac{\partial^2\bar{w}}{\partial x^2}\right)^2+\left(\frac{\partial^2\bar{w}}{\partial y^2}\right)^2\right)\\ +2D_{12}\left(\frac{\partial^2\bar{w}}{\partial x^2}\frac{\partial^2\bar{w}}{\partial y^2}\right)+4D_{66}\left(\frac{\partial^2\bar{w}}{\partial x\partial y}\right)^2\\ +k_w\left\{\bar{w}^2+\mu\left\{\left(\frac{\partial\bar{w}}{\partial x}\right)^2+\left(\frac{\partial\bar{w}}{\partial y}\right)^2\right\}\right\}\\ +k_p\begin{Bmatrix}\left(\frac{\partial\bar{w}}{\partial x}\right)^2+\left(\frac{\partial\bar{w}}{\partial y}\right)^2\\ +\mu\left(\left(\frac{\partial^2\bar{w}}{\partial x^2}\right)^2+\left(\frac{\partial^2\bar{w}}{\partial y^2}\right)^2+2\left(\frac{\partial^2\bar{w}}{\partial x\partial y}\right)^2\right)\end{Bmatrix}\end{bmatrix}dxdy \quad (23)$$

$$T=\frac{\omega^2}{2}\int_0^a\int_0^b\left[I_0\left\{\bar{w}^2+\mu\left(\left(\frac{\partial\bar{w}}{\partial x}\right)^2+\left(\frac{\partial\bar{w}}{\partial y}\right)^2\right)\right\}\right]dxdy \quad (24)$$

3.5 Hygrothermal environment

To analyze the frequency of embedded FGNP in a hygrothermal environment, two variations of moisture and temperature field across the FGNP are considered, i.e., “Uniform rise” and “Linear rise”

Table 2 SUS304/Si_3N_4 FGNP temperature dependent properties

Property	Materials	P_{-1}^T	P_0^T	P_1^T	P_2^T	P_3^T	P (T = 300K)
E (GPa)	SUS304	0	201.04	3.079×10^{-4}	-6.534×10^{-7}	0	207.7877
	Si_3N_4	0	348.43	-3.070×10^{-4}	2.160×10^{-7}	-8.946×10^{-11}	322.2715
ρ (Kg/m^3)	SUS304	0	12.330×10^{-6}	0	0	0	1.5321×10^{-6}
	Si_3N_4	0	5.8723×10^{-6}	0	0	0	7.4746×10^{-6}
α (1/K)	SUS304	0	8166	8.086×10^{-6}	0	0	8166
	Si_3N_4	0	2370	9.095×10^{-6}	0	0	2370

(i) Uniform rise:

$$T = T_0 + \Delta T; \text{ Temperature Rise (UTR)} \tag{25}$$

$$c = c_0 + \Delta c; \text{ Moisture Rise (UMR)} \tag{26}$$

where T_0, c_0, ΔT, and Δc are initial uniform temperature, initial uniform moisture, temperature change and moisture change, respectively.

(ii) Linear rise:

Temperature Rise (LTR)

$$T(z) = \frac{\Delta T}{h}\left(z + \frac{h}{2}\right) + T_{metal} \qquad \Delta T = T_{ceramics} - T_{metal} \tag{27}$$

Moisture Rise (LMR)

$$c(z) = (c_{ceramics} - c_{metal})\left(\frac{2z + h}{2h}\right) + c_{metal} \tag{28}$$

Here, $T(z)$, $c(z)$ are temperature distribution and moisture distribution respectively, through-thickness and T_{metal} = 300K. Further, the material properties in the presence of thermal environment is taken the nonlinear function of temperature as

$$P(T) = P_0^T\left(\frac{P_{-1}^T}{T} + 1 + P_{-1}^T T + P_2^T T^2 + P_3^T T^3\right) \tag{29}$$

Here, $T = T_0 + \Delta T(z)$ denotes the surrounding temperature and P_0, P_1, P_2 and P_3 are temperature co-efficients. The temperature-dependent material properties are presented in Table 2.

The stress-strain relationship of FGNP in matrix form in the presence of hygrothermal environment is given as (Lee and Kim 2013)

$$\begin{Bmatrix}\sigma_x^{nl}\\ \sigma_y^{nl}\\ \tau_{xy}^{nl}\end{Bmatrix} - (\mu\nabla^2)\begin{Bmatrix}\sigma_x^{nl}\\ \sigma_y^{nl}\\ \tau_{xy}^{nl}\end{Bmatrix} = \begin{bmatrix}C_{11} & C_{12} & 0\\ C_{21} & C_{22} & 0\\ 0 & 0 & C_{66}\end{bmatrix}\begin{Bmatrix}\varepsilon_{xx} - \alpha\Delta T - \beta\Delta c\\ \varepsilon_{yy} - \alpha\Delta T - \beta\Delta c\\ 0\end{Bmatrix} \tag{30}$$

where

$$C_{11} = C_{22} = \frac{E(z,T)}{1-\nu^2}, \qquad C_{12} = C_{21} = \frac{\nu E(z,T)}{1-\nu^2} \qquad C_{66} = \frac{E(z,T)}{2(1+\nu)} \tag{31}$$

Further, considering the temperature and moisture environment, the strain energy U_{ht} is

$$U_{ht} = -\frac{1}{2}\int_0^a\int_0^b \begin{bmatrix}\left(D_{11}^{ht} + D_{12}^{ht}\right)\begin{Bmatrix}\left(\frac{\partial^2\bar{w}}{\partial x^2}\right)^2\\ +2\left(\frac{\partial^2\bar{w}}{\partial x\partial y}\right)^2 + \left(\frac{\partial^2\bar{w}}{\partial y^2}\right)^2\end{Bmatrix}\\ +\left(A_{11}^{ht} + A_{12}^{ht}\right)\left\{\left(\frac{\partial\bar{w}}{\partial x}\right)^2 + \left(\frac{\partial\bar{w}}{\partial y}\right)^2\right\}\end{bmatrix} dxdy \tag{32}$$

where

$$\left(D_{11}^{ht}, D_{12}^{ht}\right) = \int_{-\hbar/2}^{\hbar/2}(C_{11}, C_{12})\, z^2(\alpha(z)\Delta T + \beta(z)\Delta c)dz$$
$$\left(A_{11}^{ht}, A_{12}^{ht}\right) = \int_{-\hbar/2}^{\hbar/2}(C_{11}, C_{12})\,(\alpha(z)\Delta T + \beta(z)\Delta c)dz \tag{33}$$

The effective strain energy $\left(U_{eff}\right)$ in the hygrothermal environment is

$$U_{eff} = U + U_{ht} \tag{34}$$

3.5 Rayleigh-Ritz

The Rayleigh-Ritz method with algebraic polynomial function obviates the complex work of choosing the functions to suit the edge condition. The degree of polynomials may be increased to obtain an accurate solution. Accordingly, the maximum transverse deflection is given as

$$\bar{w}(x,y) = \sum_{i=1}^{n}\varsigma_i\phi_i(x,y) \tag{35}$$

where the approximation order is n, ς_i are unknown constants, and $\phi_i(x,y)$ is an admissible function. The admissible function is defined by the product of equations of the essential edge conditions polynomials η raised to the power of χ, ι, φ and o having values either 0, 1 or 2 corresponding to free (F), simply supported (S) and clamped (C) edges, respectively and polynomials $\wp_i(x,y)$.

$$\phi_i = \eta\wp_i(x,y) \qquad i = 0,1,2,\ldots n \tag{36}$$

$$\eta = x^{\chi}y^{\iota}(x-a)^{\varphi}(y-b)^{o} \tag{37}$$

$$\wp_i(x,y) = 1, x, y, x^2, xy, y^2, x^3, x^2y, xy^2, y^3 \ldots \tag{38}$$

The Rayleigh quotient (ω^2) in a hygrothermal environment is obtained by equating effective strain energy $\left(U_{eff}\right)$ and kinetic energy (T).

$$\omega^2 = \frac{U_{eff}}{\frac{1}{2}\int_0^a\int_0^b\left[I_0\left\{\bar{w}^2 + \mu\left(\left(\frac{\partial\bar{w}}{\partial x}\right)^2 + \left(\frac{\partial\bar{w}}{\partial y}\right)^2\right)\right\}\right]dxdy} \tag{39}$$

Further, a partial derivative of ω^2 with an unknown constant is taken and equated to 0 as

$$\frac{\partial\omega^2}{\partial\varsigma_i} = 0 \qquad i = 1,2,3,4,\ldots n \tag{40}$$

On solving Eq. (40), the equation containing the stiffness and inertia matrix is obtained as

$$\{\Delta\}\left(\left[K + K_{foundation}\right]_{n\times n} - \Omega^2[M]_{n\times n}\right) = 0 \tag{41}$$

Table 3 Convergence of Ω of an embedded FGNP for k_w = 100, k_p = 100, a/b = 0.5, μ = 1 and k = 2

BC	n	1st Ω	2nd Ω	3rd Ω	4th Ω
CCCC	15	18.6606	21.6174	26.4453	31.7129
	20	18.6606	21.6159	26.4451	30.8880
	25	17.8696	19.8162	25.6269	30.7080
	30	16.7696	19.7259	24.5168	30.6983
	35	16.6596	19.6159	24.4168	30.4883
SSSS	15	10.9835	14.9942	20.5121	25.0431
	20	10.7734	14.7851	20.4210	25.9628
	25	9.9833	13.9801	19.286	22.9626
	30	8.8833	12.7701	18.2331	21.9621
	35	8.8833	12.7701	18.2331	21.9621

where Δ is a coefficient, Ω is a nondimensionalized frequency while $[K]$, $[K_{foundation}]$ and $[M]$ are a stiffness matrix, a foundation stiffness matrix and an inertia matrix, respectively. Eq. (41) is a standard eigenvalues equation, which is used for finding the frequency of the embedded FGNP. Here, the frequency is expressed in a nondimensionalized form as $\Omega = \omega a^2 \sqrt{\frac{I_c}{D_c}}$ where $I_c = \rho_c h$ and flexural rigidity is $D_c = \frac{E_c h^3}{12(1-\nu^2)}$.

4. Results and discussions

In this section, the effect of various parameters on Ω of embedded FGNP is presented and discussed subsequent to the convergence test. This section is further divided into the two subsections i.e., sections 4.1 and 4.2, depicting the vibration behavior of the embedded FGNP without and with the hygrothermal environment, respectively, along with the verification of the proposed mathematical model.

4.1 In absence of hygrothermal environment

4.1.1 Convergence

To set up the minimum required degree of the polynomials to attain the correct results, a convergence test is performed for the vibration behavior of FGNP and reported in Table 3. It is inferred from Table 3 that Ω of embedded FGNP converges to the accurate value as polynomials (n) increases to 35, and no change in frequency parameter is seen on further increase in the number of polynomials.

After the present mathematical model is successfully tested for the convergence, the accuracy of the proposed model is checked in the following subsection.

Table 5 Comparisons of the 1st Ω of SSSS FGNP for a/b = 1, b/h = 10, k_w = 100 and k_p = 0

k	μ	Source	1st Ω
0	1	Present	1.9197
		Ansari *et al*. (2016)	1.9214
	2	Present	1.7234
		Ansari *et al*. (2016)	1.7431
	3	Present	1.5750
		Ansari *et al*. (2016)	1.5961
	4	Present	1.4750
		Ansari *et al*. (2016)	1.4820
1	1	Present	1.5805
		Ansari *et al*. (2016)	1.6010
	2	Present	1.4188
		Ansari *et al*. (2016)	1.4364
	3	Present	1.3013
		Ansari *et al*. (2016)	1.3201
	4	Present	1.2066
		Ansari *et al*. (2016)	1.2211
8	1	Present	1.4366
		Ansari *et al*. (2016)	1.4560
	2	Present	1.2903
		Ansari *et al*. (2016)	1.3096
	3	Present	1.1840
		Ansari *et al*. (2016)	1.2005
	4	Present	1.0964
		Ansari *et al*. (2016)	1.1137

Table 4 Comparisons of Ω of the plate on Winkler and Pasternak substrate for μ = 0, a/b = 1

BC	Source	k_w	k_p	1st Ω	2nd Ω	3rd Ω	4th Ω	5th Ω	6th Ω
SSSS	Present	100	0	22.1277	50.3520	50.3520	79.5940	99.2245	99.2246
	Chakraverty and Pradhan (2014)	100	0	22.1277	50.3520	50.3520	79.5940	99.2245	99.2246
	Present	0	100	48.6146	-	-	-	-	140.1794
	Bahmyari *et al*. (2013)	0	100	48.6146	-	-	-	-	140.1794
SCSC	Present	100	0	30.6293	55.6498	70.0446	95.1134	102.732	129.484
	Chakraverty and Pradhan (2014)	100	0	30.6293	55.6498	70.0446	95.1134	102.732	129.484
	Present	0	100	54.7225	-	-	-	-	166.3948
	Bahmyari *et al.* (2013)	0	100	54.7225	-	-	-	-	166.3948

Table 6 Frequency parameters of embedded FGNP under 24 different BC (k = 0.5, μ = 1, a/b = 2, 1 and k_w = 100 and k_p = 200)

BCs	a/b = 2				a/b = 1			
	1st Ω	2nd Ω	3rd Ω	4th Ω	1st Ω	2nd Ω	3rd Ω	4th Ω
CCCC	48.1173	53.0503	62.3237	78.0394	19.336	28.6876	35.1087	41.1751
SSSS	26.1369	35.3744	47.6178	55.2355	13.6048	26.2147	26.2147	35.4799
FFFF	2.1623	2.16867	2.17515	11.4233	2.16234	2.1687	2.1687	9.29617
SCSC	35.7523	43.2311	54.9325	66.5217	17.9864	31.0666	31.3489	40.5337
SCSS	27.1756	37.9582	51.8532	55.5450	15.9876	27.2413	30.3589	38.4204
SCSF	13.6531	28.5426	29.6149	40.7203	12.3528	18.0381	27.7685	28.8377
SSSF	10.9447	24.4338	28.7876	38.7879	8.9094	16.2792	22.9789	27.7123
CCCS	36.7324	45.8246	58.2248	66.7792	20.9258	32.3951	35.7698	43.3882
CCSS	28.6279	41.1324	55.2799	55.9136	19.3360	28.6876	35.1087	41.1751
CCFF	16.5529	17.9030	32.4741	32.6149	16.6107	17.2636	21.5373	32.9049
CFCF	11.6440	19.6323	30.4697	34.5371	5.9201	13.6806	16.1796	23.6455
CFSF	6.5032	17.1325	25.4572	30.0345	4.8402	11.7154	14.8282	21.9302
CFFF	3.6144	8.0656	13.0385	22.3542	3.6304	6.5145	12.5415	14.8864
SSFF	7.6347	13.9228	22.0128	27.7822	7.7179	10.9724	18.3926	22.3730
SFFF	2.1644	7.1744	9.55886	20.4153	2.1644	5.2936	9.5318	13.8278
SFSC	32.9588	35.9106	42.2702	61.5245	12.3528	18.0380	27.7685	28.8377
SCCC	47.4929	51.0551	59.5393	74.2294	20.9258	32.3951	35.7698	43.3882
SCCS	35.7523	43.2311	54.9325	66.5217	17.9864	31.0666	31.3489	40.5337
CFFS	6.5032	17.1325	25.4571	30.0345	4.84	11.7154	14.8282	21.9302
CFSC	33.0041	36.7235	44.2907	57.2845	12.7369	20.0795	27.9049	32.3768
CFSS	23.0428	29.7482	40.0335	53.2102	9.5188	18.6057	23.1616	30.1293
CCCF	19.1345	33.9829	37.4495	47.3317	17.0268	22.1483	33.0409	33.5210
CSCF	16.3877	29.5894	36.8277	44.7012	12.7369	20.0795	27.9049	32.3768
SFSF	5.2841	14.7672	24.4681	27.0997	3.5176	10.6767	12.2566	20.3216

4.1.2 Comparison

The Ω of the isotropic plate on the Winkler and Pasternak substrate subjected to different boundary constraints are matched with published results (Tables 4 and 5). The obtained results vary nominally (about 1.1%) for μ = 4 and k = 8 (Table 5) from the results of Ansari *et al*. (2016), who used the GDQ method for solving the vibration problem. Although the GDQ method is straightforward but when mixed edge constraints are considered, it becomes very challenging since only one quadrature equation at one point is possible.

It is evident from this section that the proposed model is valid for the FGNP without a hygrothermal environment. After the convergence and validation test, new results are presented and discussed in subsection 4.1.3.

4.1.3 Parameters' effect

Initial five Ω of FGNP under 24 different mixed BCs for a/b = 1 and 2 are tabulated in Table 6. The Ω of clamped embedded FGNP is highest, whereas free embedded FGNP has the lowest Ω for both square and the rectangular plates (Table 6). This kind of behavior is observed because the more the constraints are imposed on the edges of the plate, the higher will be the stiffness and hence the non-dimensional frequencies ($\Omega_{CCCC} > \Omega_{SSSS} > \Omega_{FFFF}$).

Table 7 Frequency parameters of embedded FGNP w.r.t μ and a/b for k = 1, k_W = 50 and k_p = 50

a/b	μ	1st Ω			
		CCCC	CFSF	SFSC	SSSS
0.5	0	21.6267	3.8630	4.7763	10.9373
	1	17.0718	3.5728	4.3555	8.9936
	2	14.5400	3.34927	4.0402	8.7449
	4	11.6893	3.0273	3.5955	6.6476
1	0	31.6218	4.5491	14.8316	17.3932
	1	22.5379	4.2452	11.8208	13.0423
	2	18.4344	3.8816	10.1081	10.8976
	4	14.3088	3.3881	8.1586	8.7721
2	0	86.3001	7.6317	55.2554	49.4401
	1	46.3723	6.0866	31.6720	25.1628
	2	35.3922	5.4653	24.4086	19.5326
	4	26.1310	4.5282	18.0764	14.6856

The fundamental nondimensionalized frequency (1st Ω)

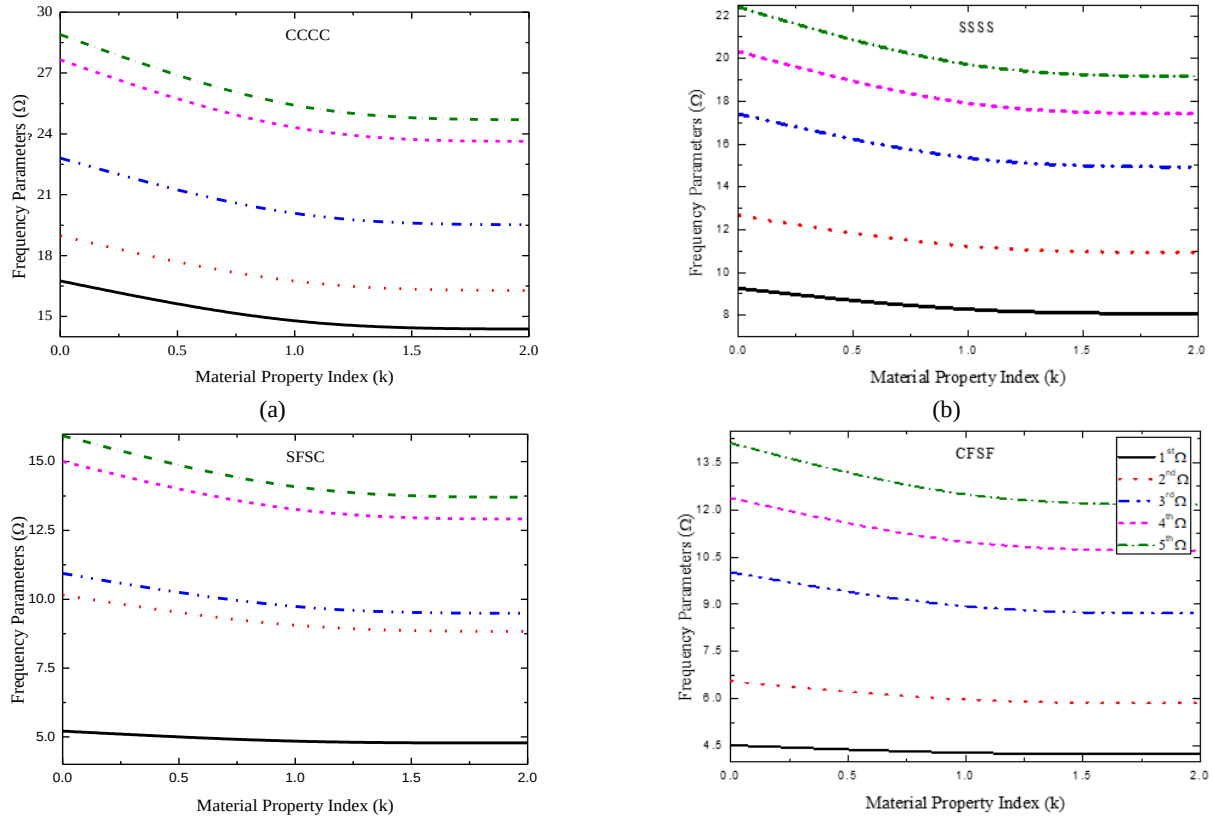

Fig. 3 Variation of Ω of embedded FGNP with k for $\mu = 2$, $a/b = 0.5$, $k_w = 200$ and $k_p = 100$

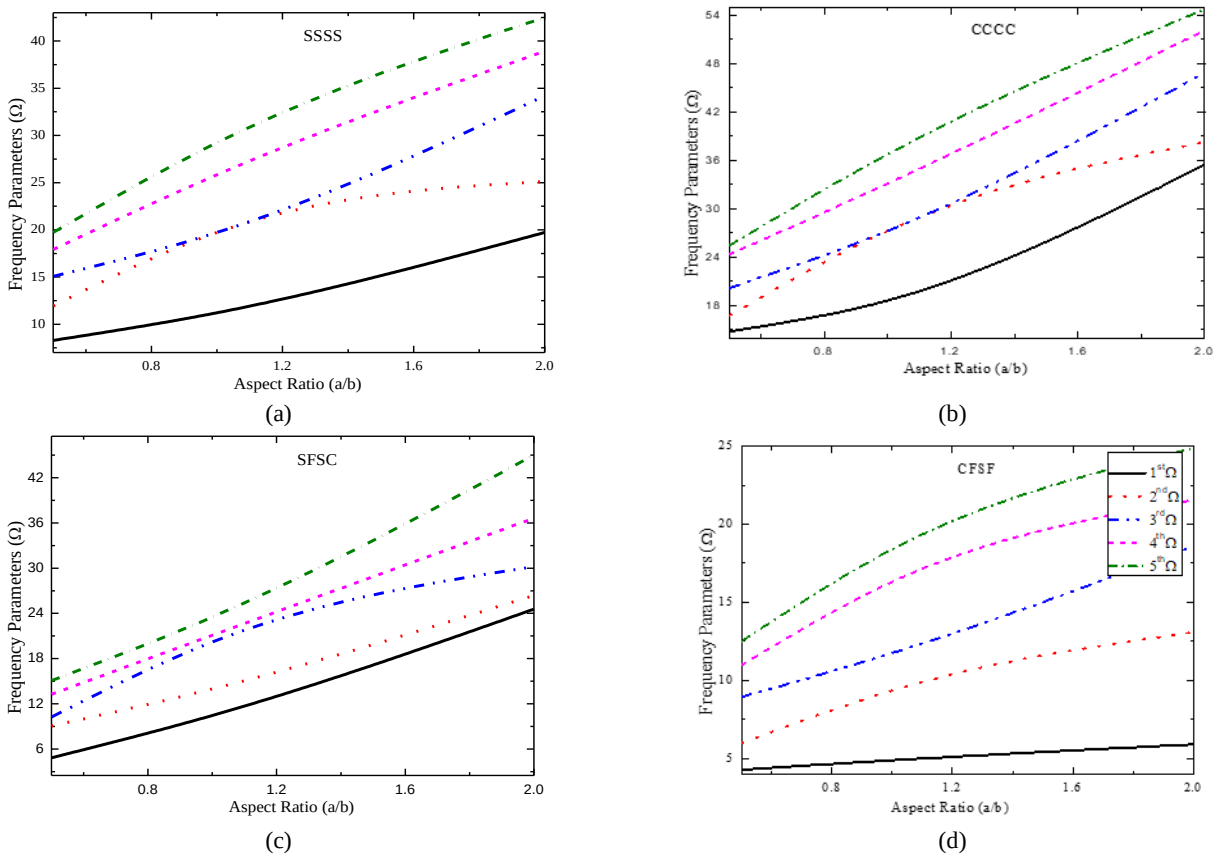

Fig. 4 Variation of Ω of embedded FGNP with a/b for $\mu = 2$, $k = 1$, $k_w = 200$ and $k_p = 100$

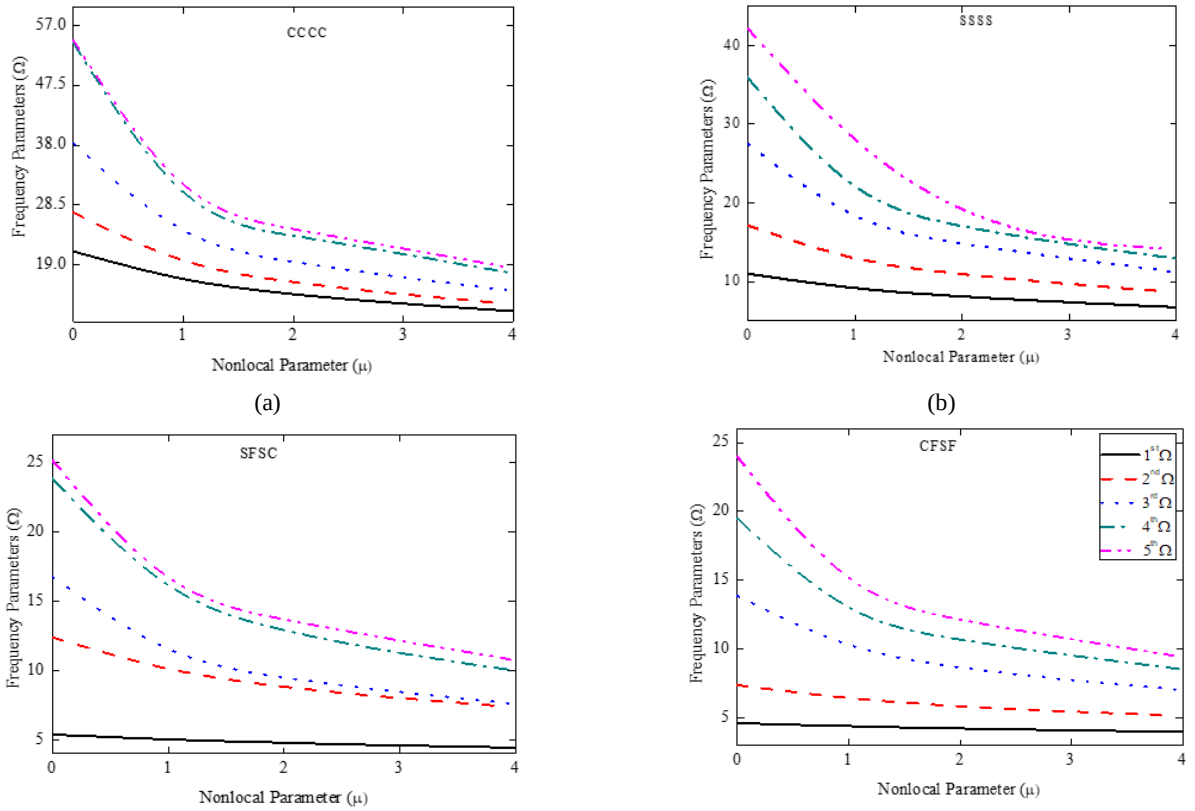

Fig. 5 Variation of Ω of embedded FGNP with μ for k = 1, a/b =0.5, k_w = 200 and k_p = 100

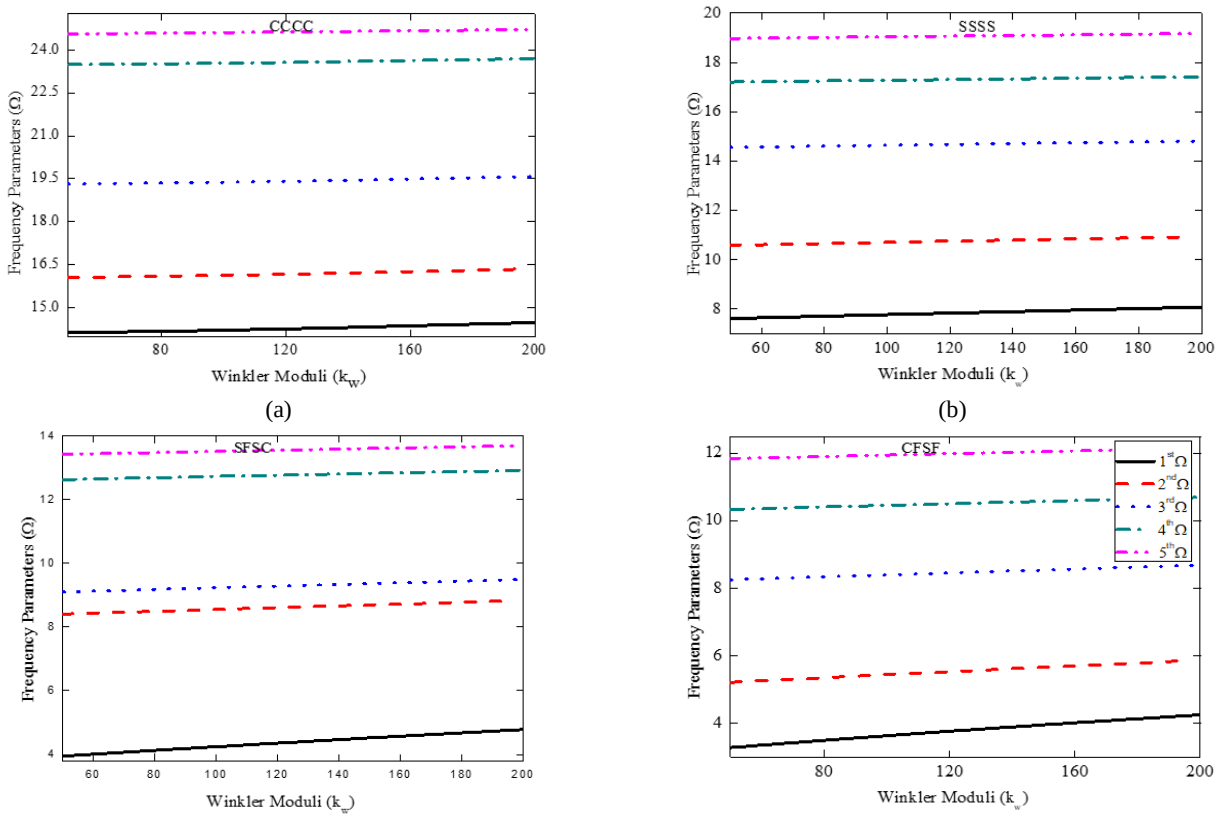

Fig. 6 Effect of k_w on Ω of embedded FGNP for k = 1, μ = 2, a/b = 0.5 and k_p = 200

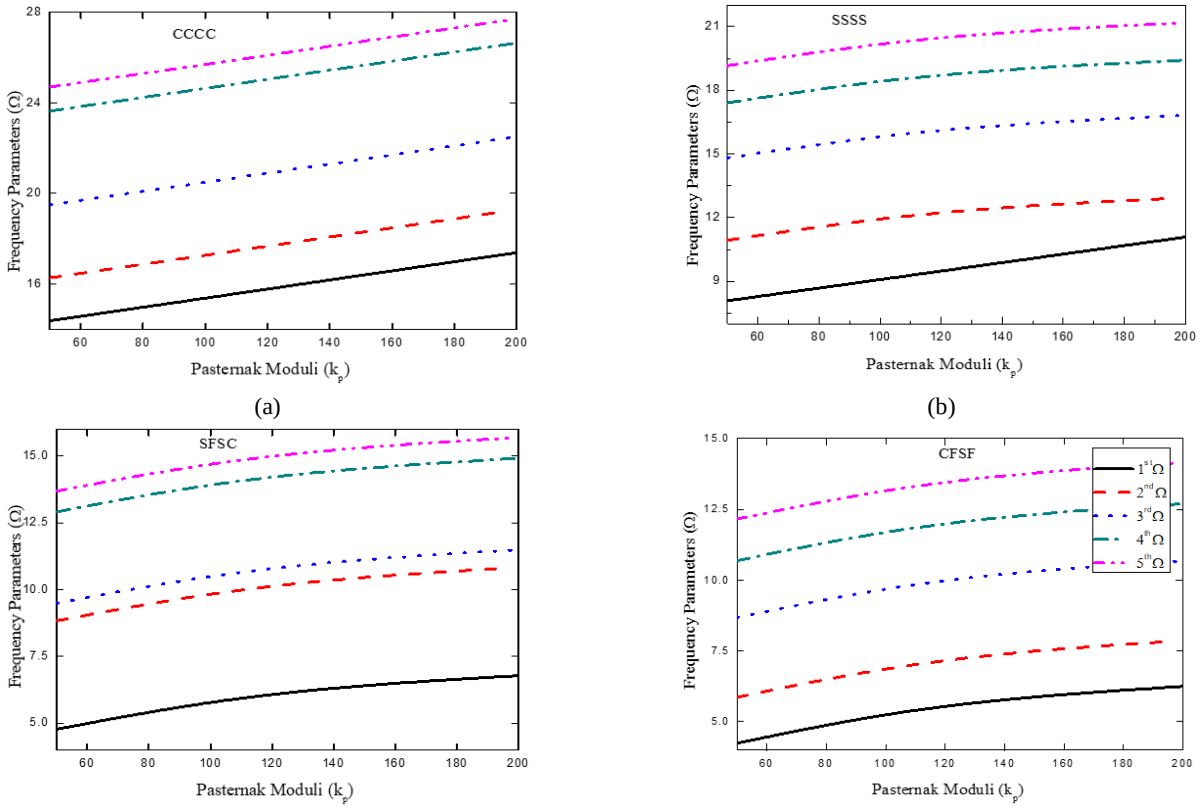

Fig. 7 Effect of k_p on Ω of embedded FGNP for k = 1, μ = 2, a/b = 0.5 and k_w = 200

Table 8 Comparison of Ω of simply supported FGNP for a/b = 1, μ = 0, ΔT = 300

k		Source	CCCC					SSSS				
			1st Ω	2nd Ω	3rd Ω	4th Ω	5th Ω	1st Ω	2nd Ω	3rd Ω	4th Ω	5th Ω
1	Uniform rise	Present	4.086	8.1179	8.1179	11.5102	13.566	2.4501	6.0751	6.0751	8.6523	8.6523
		Yang and Shen (2002)	4.2110	8.2429	8.2429	11.6602	13.716	2.5511	6.1761	6.1761	8.7623	8.7623
	Linear rise	Present	4.3556	7.5556	7.5556	11.9887	14.1787	2.5533	6.2692	6.2692	8.8548	8.8548
		Yang and Shen (2002)	4.4806	7.6806	7.6806	12.1387	14.3287	2.6543	6.3702	6.3702	8.9648	8.9648
2	Uniform rise	Present	3.5952	7.176	7.176	10.1848	12.0756	2.168	5.3974	5.3974	7.6131	7.6131
		Yang and Shen (2002)	3.7202	7.3010	7.3010	10.3348	12.2256	2.2690	5.4984	5.4984	7.7231	7.7231
	Linear rise	Present	3.8608	6.7875	6.7875	10.6582	12.5939	2.2678	5.5848	5.5848	7.8143	7.8143
		Yang and Shen (2002)	3.9858	6.9125	6.9125	10.8082	12.7439	2.3688	5.6858	5.6858	7.9243	7.9243

of the embedded FGNP with a/b and μ for different BC is presented in Table 7. 1st Ω increases with a/b but decreases with nonlocal effect. Relative Percentage Change (RPC), expressed by Eq. (43), highlights the importance of the nonlocal effect for FGNP with high aspect ratios.

$$RPC = \frac{\Omega_{Local} - \Omega_{Nonlocal}}{\Omega_{Local}} \tag{42}$$

The RPC goes on increasing with a/b and/or μ. For example, a/b = 0.2 and 2 with μ = 2, the RPC is 38.7241%

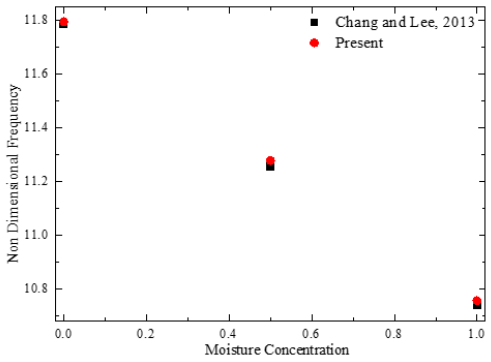

Fig. 8 Nondimensional fundamental frequencies of rectangular plate with moisture

and 64.1028% respectively for a clamped FGNP. This rise in the RPC shows that overpredicted frequencies are computed using local elasticity theory. Hence, the nonlocal effect must be considered for a reliable and accurate design of nanostructures.

The effect of parameters viz. aspect ratio, material property exponent, nonlocal parameter, and foundation on Ω of Al/ZrO_2 embedded FGNP have been analyzed in this section. The frequency parameters of the embedded FGNP w.r.t. material property index is presented in Fig. 3. It is seen that the Ω decrease with increasing k irrespective of BC. This is because, with an increase in k, the percentage of metal constituent increases in FGNP, which reduces the stiffness of the plate, leading to decrease in Ω.

Table 9 Ω of CCCC SUS304/Si_3N_4 embedded FGNP (T = 300K, k_w = 100 and k_p = 200)

μ	k	a/b	Δc	ΔT	Uniform rise				Linear rise			
					1st Ω	2nd Ω	3rd Ω	4th Ω	1st Ω	2nd Ω	3rd Ω	4th Ω
1	1	0.5	0.25	300	10.4907	13.7086	29.1941	32.2395	10.5761	13.8031	29.2950	32.3495
				500	10.1707	13.3886	28.8741	31.9195	10.3178	13.5411	29.0457	32.1106
			0.75	300	8.6058	11.5484	26.9407	29.8332	8.6913	11.6428	27.0417	29.9431
				500	8.3060	11.2485	26.6409	29.5334	8.4532	11.4010	26.8125	29.7244
		1	0.25	300	3.9275	8.3369	8.3369	12.2911	4.0130	8.43142	8.43142	12.4010
				500	3.8856	8.2853	8.2853	12.2313	3.8328	8.03247	8.03247	12.0144
			0.75	300	3.4276	7.7389	7.7389	11.6027	3.5131	7.83345	7.83345	11.7127
				500	3.3793	7.6833	7.6833	11.5395	3.2673	7.3501	7.3501	11.0553
	2	0.5	0.25	300	9.4213	12.3128	26.2348	28.9721	9.5160	12.4249	26.3623	29.1031
				500	9.2693	12.1361	26.0438	28.7678	9.4249	12.3145	26.2475	28.9874
			0.75	300	7.7431	10.3889	24.2231	26.8234	7.8378	10.5009	24.3506	26.9545
				500	7.5556	10.1787	24.0161	26.6027	7.7111	10.3572	24.2198	26.8223
		1	0.25	300	3.5283	7.4921	7.4921	11.0467	3.6297	7.6144	7.6144	11.1791
				500	3.3183	7.2821	7.2821	10.8367	3.4911	7.4641	7.4641	11.0298
			0.75	300	3.0828	6.9580	6.9580	10.4311	3.1842	7.0804	7.0815	10.5635
				500	2.9118	6.7870	6.7870	10.2601	3.0846	6.9691	6.9691	10.4533
2	1	0.5	0.25	300	10.033	13.2511	28.7365	31.7819	10.0946	13.3233	28.8120	31.8741
				500	9.7130	12.9310	28.4165	31.4619	9.8141	12.9522	28.4510	31.4964
			0.75	300	8.1482	11.0908	26.4831	29.3756	8.2097	11.1630	26.5586	29.4677
				500	7.8484	10.7909	26.1833	29.0758	7.9495	10.8121	26.2178	29.1102
		1	0.25	300	3.5225	7.9319	7.9319	11.8861	3.6680	8.0943	8.0943	12.0782
				500	3.4806	7.8803	7.8803	11.8263	3.6261	8.0427	8.0427	12.0185
			0.75	300	3.0226	7.3339	7.3339	11.1977	3.1682	7.4963	7.4963	11.3899
				500	2.9743	7.2783	7.2783	11.1345	3.1198	7.4407	7.4407	11.3266
	2	0.5	0.25	300	9.1908	12.0823	26.0043	28.7415	9.2019	12.2047	26.0367	29.0746
				500	9.0388	11.9055	25.8133	28.5373	9.1530	12.0279	25.8454	28.8494
			0.75	300	7.5126	10.1584	23.9926	26.5929	7.5237	10.2807	24.0247	26.9260
				500	7.3251	9.9482	23.7856	26.3722	7.4393	10.0706	23.8177	26.6843
		1	0.25	300	3.2978	7.2616	7.2616	10.8162	3.4348	7.4136	7.4136	10.9939
				500	3.0878	7.0515	7.0515	10.6062	3.2248	7.2036	7.2036	10.7838
			0.75	300	2.8523	6.7275	6.7275	10.2006	2.9893	6.8796	6.8796	10.3783
				500	2.6813	6.5565	6.5565	10.0296	2.8184	6.7086	6.7086	10.2073

Table 10 Ω of SSSS SUS304/Si_3N_4 embedded FGNP (T = 300K, k_w = 100 and k_p = 200)

μ	k	a/b	Δc	ΔT	Uniform rise				Linear rise			
					1st Ω	2nd Ω	3rd Ω	4th Ω	1st Ω	2nd Ω	3rd Ω	4th Ω
1	1	0.5	0.25	300	4.0651	7.6238	17.9455	18.0529	4.1863	7.7665	18.097	18.2036
				500	3.7616	7.364	17.732	17.8062	3.9127	7.5268	17.9042	17.9768
			0.75	300	3.8171	6.6238	15.3862	17.0529	4.0594	6.9093	15.6905	17.3542
				500	3.2675	6.364	15.1366	16.8062	3.4187	6.5268	15.3088	16.9768
		1	0.25	300	2.9012	5.3719	5.3719	10.3982	3.0445	5.5222	5.5222	10.5469
				500	2.8362	5.3097	5.3097	10.3357	2.8246	5.1003	5.1003	10.4101
			0.75	300	1.9461	4.6278	4.6278	9.6736	2.2326	4.9284	4.9284	9.9710
				500	1.8073	4.5555	4.5555	9.606	1.9782	4.8058	4.8058	9.8662
	2	0.5	0.25	300	3.6342	6.8364	16.1198	16.2141	3.7864	6.9996	16.2971	16.4028
				500	3.3311	6.5786	15.9088	15.9701	3.5034	6.7618	16.0860	16.1353
			0.75	300	3.4535	13.5500	13.8398	21.3279	3.6057	13.7128	14.0171	21.5161
				500	2.9101	13.2571	13.5936	21.0798	3.0823	13.4399	13.7708	21.2450
		1	0.25	300	1.7048	4.8255	4.8255	9.3446	1.9572	5.0983	5.0983	9.6769
				500	1.6403	4.7641	4.7641	9.2830	1.8634	5.1475	5.1475	9.8352
			0.75	300	1.5624	4.1626	4.1626	8.6974	1.5826	4.4354	4.4354	9.0297
				500	1.3718	4.0912	4.0912	8.63121	1.4119	4.4746	4.4746	9.1834
2	1	0.5	0.25	300	3.9109	7.4696	17.7913	17.8987	3.9663	7.5363	17.8658	17.9737
				500	3.6074	7.2098	17.5778	17.652	3.7628	7.3765	17.7524	18.0697
			0.75	300	3.6629	6.4696	15.2320	16.8987	3.7182	6.5363	15.3065	16.9763
				500	3.1133	6.2098	14.9824	16.652	3.2688	6.3765	15.1571	17.0697
		1	0.25	300	2.7058	5.1764	5.1765	10.2027	2.9649	5.4210	5.4210	10.9879
				500	2.6407	5.1143	5.1143	10.1402	2.7413	5.1142	5.1142	10.1402
			0.75	300	1.2313	4.4324	4.4324	9.4782	2.0097	4.6769	4.6769	10.2633
				500	1.1127	4.3610	4.3601	9.4109	1.6119	4.3600	4.3600	9.4109
	2	0.5	0.25	300	3.4298	6.6320	15.9154	16.0096	3.6889	6.8765	16.1599	16.7948
				500	3.1267	6.3742	15.7044	15.7657	3.3858	6.6187	15.9489	16.5509
			0.75	300	3.2491	13.3451	13.6354	21.1235	3.5082	13.5898	13.8799	21.9087
				500	2.7056	13.0520	13.3891	20.8754	2.9648	13.2969	13.6341	21.6605
		1	0.25	300	1.4504	4.5711	4.5711	9.0902	1.7096	4.8156	4.8156	9.8753
				500	1.3859	4.5096	4.5097	9.0286	1.6450	4.7542	4.7542	9.8138
			0.75	300	1.0136	3.9082	3.9082	8.4430	1.5607	4.1527	4.1527	9.2282
				500	0.8645	3.8368	3.8368	8.3768	1.4056	4.0813	4.0813	9.1629

The trend of variation in natural frequencies of the embedded FGNP with a/b has been plotted in Fig. 4. Analysis of the figure indicates that Ω increases on increasing a/b. This is because, on increasing a/b for a specified edge length, one of the edges of FGNP becomes small leading to a decrease in the plate's size, which causes an increase in stiffness of the FGNP in turn, increases Ω. It is also seen that 2nd Ω and 3rd Ω of a clamped square FGNP is identical (2nd Ω = 3rd Ω). This same behavior holds for the case of simply supported edge constraints. This is because of the symmetricity of the edge conditions governing polynomials of CCCC and SSSS square FGNP. However, such behavior is not shown by a rectangular plate ($a/b \neq 1$).

Further, the small-scale effect on Ω of embedded FGNP is shown in Fig. 5. It is evident from the figure that Ω is highest for μ = 0 and goes on decreasing as the nonlocal effect increases. It is attributed to the fact that springs linking the atoms are considered to have infinite spring constant in the local model, whereas the nonlocal model is seen as an elastic spring linking the atom, which makes the nano FG plate more flexible. The nonlocal effect is observed to be prominent for the higher modes.

Furthermore, the variation of Ω with Winkler (k_w) and Pasternak (k_p) moduli is plotted in Figs. 6 and 7, respectively. Ω increases by either increasing k_w or k_p irrespective of the BCs, but the rate of increase in Ω for both the cases is different. Ω increases very nominally when k_w is increased, whereas Ω increases monotonically with a

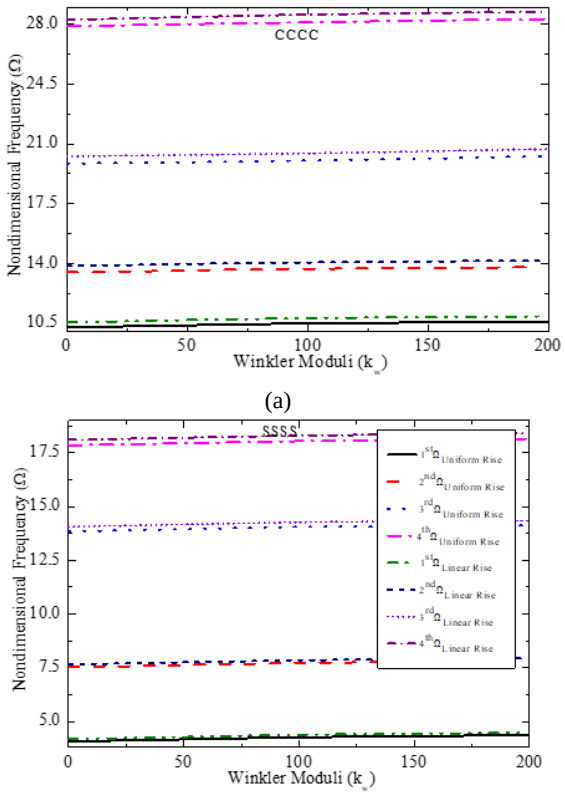

Fig. 9 Winkler moduli influence on Ω of SUS304/Si_3N_4 embedded FGNP (a/b = 0.5, μ = 1, k = 1, k_p = 100, Δc = 0.25, ΔT =300K)

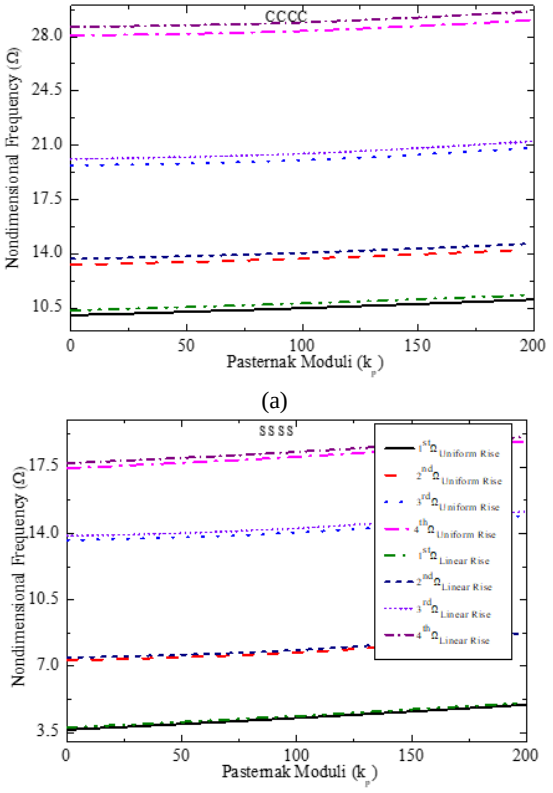

Fig. 10 Pasternak moduli effect on Ω of SUS304/Si_3N_4 embedded FGNP (a/b = 0.5, μ = 1, k = 1, k_w = 100, Δc = 0.25, ΔT = 300K)

rise in the shear effect (k_p). The reason is that, increasing the stiffness of the foundation stiffens the support, leading to an increase in Ω.

4.2 In hygrothermal environment

4.2.1 Comparison

This section deals with the vibration characteristic of FGNP in the hygral and thermal environment. For validating the computed frequencies in the hygrothermal environment, firstly, we have computed results for FGM plate in the thermal environment and are compared with the results of existing literature (Table 8) as scarce work in this regard is available.

Secondly, the comparison of frequencies in a hygral environment is done with the previously published results (Lee and Kim 2013) and plotted in Fig. 8. Results are seen to be almost similar (Fig. 8) having a percentage difference of about 1.08%, 1.4% and 1.8% for c = 0, 0.5 and 1, respectively. The reason for this small variation in the result is a difference in the methodology used, Lee and Kim have employed the FSDT with Newton Rapson while Rayleigh-Ritz with CPT has been used in the present study.

It is evident from this section that the proposed model is valid for a hygrothermal environment. After the validation test, new results are reported and discussed in section 4.2.2 for embedded SUS304/Si_3N_4 FGNP in the presence of moisture and temperature.

4.2.2 Parameters' effect

In the present section effect of different parameters viz. aspect ratios, material exponent, nonlocal parameter, foundation, temperature, and moisture on non-dimensionalized frequencies of SUS304/Si_3N_4 embedded FGNP under thermal and moisture environments are reported in Tables 9 and 10. For the analysis, two different BCs are considered as SSSS and CCCC.

From the tables, Ω of the embedded SUS304/Si_3N_4 FGNP is seen decreasing on increasing k. This is due to the fact that, on increasing k, the properties of FGNP tend toward metal. Moreover, the coefficients of expansion (α, β) of metal contribute to further decrease in stiffness of FGNP. Also, it is seen that the nondimensionalized frequency of the FGNP decreases with moisture concentration and temperature. This is because, with a rise in the moisture and temperature, the plate loses it' s stiffness, thereby reducing the frequency. One more reason; the stiffness of FGNP is governed through the hygro-thermoelastic relation, which in turn affects the frequency considerably. It is noteworthy that moisture concentration has a nominal effect on Ω of embedded FGNP.

Generally, the Ω of FGNP is found to be increased on increasing a/b, but in the hygrothermal environment, Ω of FGNP decreases on increasing a/b. With an increase in a/b, for the specified edge length, the plate size decreases, causing an increase in plate stiffness. On the other hand, the presence of moisture and temperature reduces the stiffness

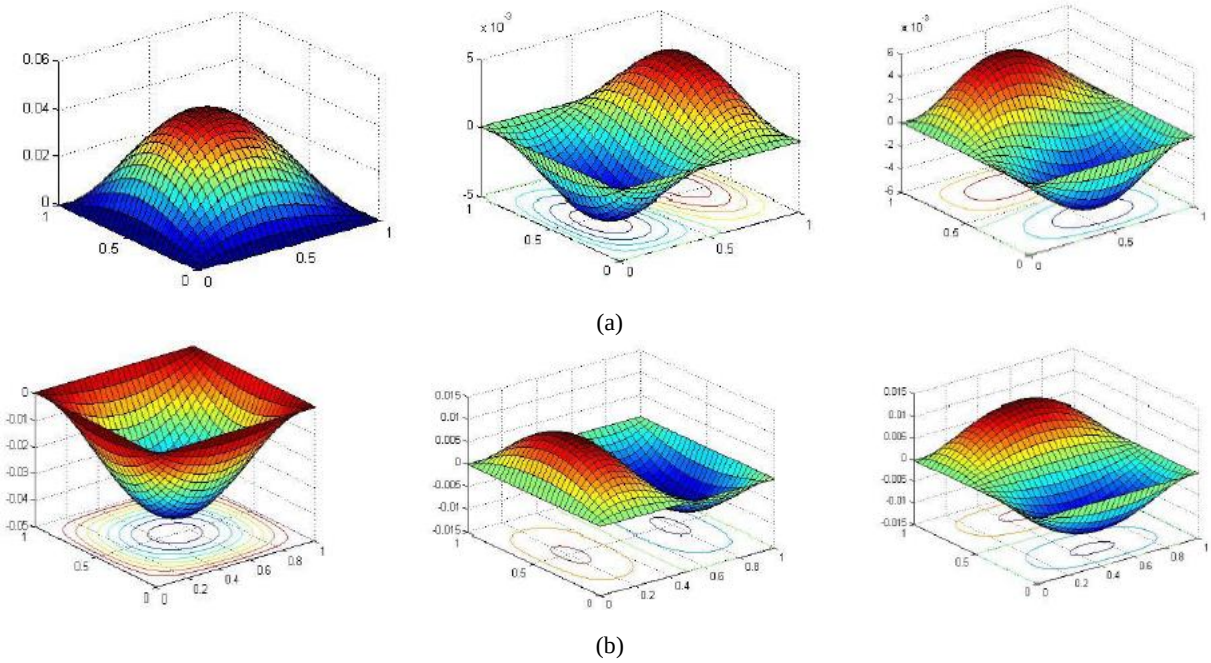

Fig. 11 Mode shapes of embedded FGNP having $k = 1$, $\mu = 1$, $a/b = 1$, $k_w = 100$, $k_p = 200$, $\Delta c = 75$, $\Delta T = 300$ for (a) simply supported edge; (b) clamped edge

of the plate. In this case, change (decrease) in Ω due to the combined effect of moisture concentration and temperature supersedes the change (increase) in Ω due to an increase in a/b and, as a result, the overall stiffness of the plate decreases. Consequently, the frequency of embedded FGNP decreases.

The effect of variation of foundation moduli on Ω of embedded FGNP in the hygrothermal environment is studied further in this section. For this, the Winkler Pasternak type foundation is considered and the computed results are depicted graphically in Figs. 9 and 10.

From the figures, it is seen that Ω increases gradually with an increase in Winkler modulus, while a monotonic increase in Ω is observed of the increasing shear effect. The reason attributing for such behavior is, increase in the coefficient of the foundation stiffens the support, causing an increase in FGNP's frequency. On comparing Figs. 9 and 10, the effect of the Pasternak modulus is found to be more pronounced than that of the Winkler modulus.

Further different mode shapes of SSSS and CCCC embedded FGNP in the hygrothermal environment are presented in Fig. 11. From figures, it is seen that although 2nd Ω and 3rd Ω of SSSS square FGNP is identical (2nd Ω = 3rd Ω) but their respected mode shapes are different. Similar behavior is observed in clamped square FGNP in a hygrothermal environment as well. It is observed that the vibration of the clamped plate is bonded to a small area that too towards the center of the FG plate. This is because of the high constraints imposed at the boundaries due to clamped edges.

5. Conclusions

In this study, the analysis of free vibration of embedded FGNP under the various combinations of mixed BCs with and without hygrothermal effect have been studied employing nonlocal classical plate theory. For the study, two different types of moisture and temperature rise are considered viz. uniform rise and linear rise. The properties of the plate material are considered to be varying following the power law. The Rayleigh-Ritz method has been implemented to compute Ω. Algebraic polynomials are used to express the displacement components. The entire computation has been carried out in MATLAB.

A detailed study on the vibration of FGNP has been conducted by varying aspect ratios, nonlocal parameter, foundation modulus, temperature and moisture concentration. The new results have been reported in tables and figures after the test of convergence and comparative study. The major outcomes of the study are reported under the following two subsections.

5.1 Notes on methodology

The presented methodology employs the Rayleigh-Ritz method with algebraic polynomials to compute the frequencies of embedded FGNP in the hygrothermal environment. Some methods highlighted in the introduction are insufficient in handling mixed edge conditions and are limited to homogeneous BCs only. The present proposed method is capable of overcoming these drawbacks as it can handle any combinations of BC easily and accurately. The major consequences of employing the proposed methods are:

• The essential edge conditions need to be satisfied in place of considering natural edge conditions.

• A lower number of polynomials are required in the present method to obtain the solution whereas a large set of trigonometric terms are needed in the Trigonometric Ritz

method. Moreover, the present method is easier compared to other methods; in the Chebyshev-Ritz method, the Chebyshev polynomials give a solution of eigenvalue problem only in the closed interval [-1, 1]. In *kp*-Ritz method, the tedious task of obtaining kernel particle's shape function and its correction is involved.

• The proposed computational model can handle any possible combinations of edge constraints without any limitations efficiently even in the presence of complex external environment.

5.2 Notes on results

The computed Ω of embedded FGNP are in accord with the published research. Interestingly the comparison of Ω of embedded FGNP with closed-form solution available in the literature reveals that the present method gives precise results.

The following conclusions can be drawn with regard to the presented results.

• With the increase in a/b, Ω of embedded FGNP increases monotonically; however, this behavior is contradicted when the analysis is conducted in the hygrothermal environment.

• The increase in material property index (k) causes a decrease in Ω of embedded FGNP. This behavior holds irrespective of the environment and edge constraints of the embedded FGNP.

• On increasing the coefficient of elastic substrate (k_w, k_p), Ω of embedded FGNP increases. Further the effect of stiffness of the Pasternak foundation (k_p) is more prominent in comparison to that of k_w.

• The nonlocal effect is significant at a higher aspect ratio of the FG nanoplate. For e.g., Relative percentage change of the frequency parameter of simply supported FGNP (μ = 2) with a/b = 0.2 and a/b = 2 is 38.7241% and 64.1028%, respectively.

• Comparing effect of temperature and moisture later has less effect on the Ω of embedded FGNP.

Lastly, the contribution of the present study lies in presenting the method to compute Ω and mode shapes of FGNP in the hygrothermal environment under mixed BCs resting on an elastic foundation, with ease and a high degree of accuracy.

Acknowledgments

The research described in this paper was not financially supported by any organization or person.

References

Adali, S. (2009), "Variational principles for transversely vibrating multiwalled carbon nanotubes based on nonlocal Euler-Bernoulli beam model", *Nano Lett.*, **9**, 1737-1741. https://doi.org/10.1021/nl8027087.

Addou, F.Y., Meradjah, M., Bousahla, A.A., Benachour, A., Bourada, F., Tounsi, A. and Mahmoud, S.R. (2019), "Influences of porosity on dynamic response of FG plates resting on Winkler/Pasternak/Kerr foundation using quasi 3D HSDT", *Comput. Concrete, Int. J.*, **24**(4), 347-367. https://doi.org/10.12989/cac.2019.24.4.347.

Aksencer, T. and Aydogdu, M. (2011), "Levy type solution method for vibration and buckling of nanoplates using nonlocal elasticity theory", *Physica E Low Dimens. Syst. Nanostruct.*, **43**(4), 954-959. https://doi.org/10.1016/j.physe.2010.11.024.

Al-Furjan, M.S.H., Safarpour, H., Habibi, M., Safarpour, M. and Tounsi, A. (2020), "A comprehensive computational approach for nonlinear thermal instability of the electrically FG-GPLRC disk based on GDQ method", *Eng. Comput.*, **2020**, 1-18. https://doi.org/10.1007/s00366-020-01088-7.

Analooei, H.R., Azhari, M. and Heidarpour, A. (2013), "Elastic buckling and vibration analyses of orthotropic nanoplates using nonlocal continuum mechanics and spline finite strip method", *Appl. Math.*, **37**(10-11), 6703-6717. https://doi.org/10.1016/j.apm.2013.01.051.

Anjomshoa, A. (2013), "Application of Ritz functions in buckling analysis of embedded orthotropic circular and elliptical micro/nanoplates based on nonlocal elasticity theory", *Meccanica*, **48**, 1337-1353. https://doi.org/10.1007/s11012-012-9670-y.

Ansari, R., Shahabodini, A. and Shojaei, M.F. (2016), "Nonlocal three-dimensional theory of elasticity with application to free vibration of functionally graded nanoplates on elastic foundations", *Physica E*, **76**, 70-81. https://doi.org/10.1016/j.physe.2015.09.042.

Asghar, S., Naeem, M.N., Hussain, M., Taj, M. and Tounsi, A. (2020), "Prediction and assessment of nonlocal natural frequencies of DWCNTs: Vibration analysis", *Comput. Concrete, Int. J.*, **25**(2), 133-144. https://doi.org/10.12989/cac.2020.25.2.133.

Bahmyari, E., Banatehrani, M.M., Ahmadi., M. and Bahmyari, M. (2013), "Vibration analysis of thin plates resting on Pasternak foundations by element free Galerkin method", *Shock Vib.*, **20**, 309-326. https://doi.org/10.3233/SAV-2012-00746.

Balubaid, M., Tounsi, A., Dakhel, B. and Mahmoud, S.R. (2019), "Free vibration investigation of FG nanoscale plate using nonlocal two variables integral refined plate theory", *Comput. Concrete, Int. J.*, **24**(6), 579-586. https://doi.org/10.12989/cac.2019.24.6.579.

Barati, M.R. (2017), "Nonlocal-strain gradient forced vibration analysis of metal foam nanoplates with uniform and graded porosities", *Adv. Nano Res., Int. J.*, **5**(4), 393-414. http://dx.doi.org/10.12989/anr.2017.5.4.393.

Barati, M.R. (2018), "Nonlocal stress-strain gradient vibration analysis of heterogeneous double-layered plates under hygro-thermal and linearly varying in-plane loads", *J. Vib. Control*, **24**(19), 4630-4647. ttps://doi.org/10.1177/1077546317731672.

Bedia, W.A., Houari, M.S.A., Bessaim, A., Bousahla, A.A., Tounsi, A., Saeed, T. and Alhodaly, M.S. (2019), "A new hyperbolic two-unknown beam model for bending and buckling analysis of a nonlocal strain gradient nanobeams", *J. Nano Res.*, **57**, 175-191. https://doi.org/10.4028/www.scientific.net/JNanoR.57.175.

Belkorissat, I., Houari, M.S.A., Tounsi, A., Bedia, E.A. and Mahmoud, S.R. (2015), "On vibration properties of functionally graded nanoplate using a new nonlocal refined four variable model", *Steel Compos. Struct., Int. J.*, **18**(4), 1063-1081. https://doi.org/10.12989/scs.2015.18.4.1063.

Bellal, M., Hebali, H., Heireche, H., Bousahla, A.A., Tounsi, A., Bourada, F., Mahmoud, S.R., Bedia, E.A. and Tounsi, A. (2020), "Buckling behavior of a single-layered graphene sheet resting on viscoelastic medium via nonlocal four-unknown integral model", *Steel Compos. Struct., Int. J.*, **34**(5), 643-655. https://doi.org/10.12989/scs.2020.34.5.643.

Bendaho, B., Belabed, Z., Bourada, M., Benatta, M.A., Bourada, F. and Tounsi, A. (2019), "Assessment of new 2D and quasi-3D nonlocal theories for free vibration analysis of size-dependent functionally graded (FG) nanoplates", *Adv. Nano Res., Int. J.*, **7**(4), 277-292. https://doi.org/10.12989/anr.2019.7.4.277.

Bensaid, I., Bekhadda, A. and Kerboua, B. (2018), "Dynamic analysis of higher order shear-deformable nanobeams resting on elastic foundation based on nonlocal strain gradient theory", *Adv. Nano Res., Int. J.*, **6**(3), 279-298. https://doi.org/10.12989/anr.2018.6.3.279.

Bensaid, I., Daikh, A.A. and Drai, A. (2020), "Size-dependent free vibration and buckling analysis of sigmoid and power law functionally graded sandwich nanobeams with microstructural defects", *Proc. Inst. Mech. Eng. C J. Mech. Eng. Sci.*, 0954406220916481. https://doi.org/10.1177/0954406220916481.

Berghouti, H., Adda Bedia, E.A., Benkhedda, A. and Tounsi, A. (2019), "Vibration analysis of nonlocal porous nanobeams made of functionally graded material", *Adv. Nano Res., Int. J.*, **7**(5), 351-364. https://doi.org/10.12989/anr.2019.7.5.351.

Bouadi, A., Bousahla, A.A., Houari, M.S.A., Heireche, H. and Tounsi, A. (2018), "A new nonlocal HSDT for analysis of stability of single layer graphene sheet", *Adv. Nano Res., Int. J.*, **6**(2), 147-162. https://doi.org/10.12989/anr.2018.6.2.147.

Bourada, F., Bousahla, A.A., Tounsi, A., Bedia, E.A., Mahmoud, S.R., Benrahou, K.H. and Tounsi, A. (2020), "Stability and dynamic analyses of SW-CNT reinforced concrete beam resting on elastic-foundation", *Comput. Concrete, Int. J.*, **25**(6), 485-495. https://doi.org/10.12989/cac.2020.25.6.485.

Bousahla, A.A., Bourada, F., Mahmoud, S.R., Tounsi, A., Algarni, A., Bedia, E.A. and Tounsi, A. (2020), "Buckling and dynamic behavior of the simply supported CNT-RC beams using an integral-first shear deformation theory", *Comput. Concrete, Int. J.*, **25**(2), 155-166. https://doi.org/10.12989/cac.2020.25.2.155.

Boussoula, A., Boucham, B., Bourada, M., Bourada, F., Tounsi, A., Bousahla, A.A. and Tounsi, A. (2020), "A simple nth-order shear deformation theory for thermomechanical bending analysis of different configurations of FG sandwich plates", *Smart Struct. Syst., Int. J.*, **25**(2), 197-218. https://doi.org/10.12989/sss.2020.25.2.197.

Boutaleb, S., Benrahou, K. H., Bakora, A., Algarni, A., Bousahla, A.A., Tounsi, A. and Mahmoud, S.R. (2019), "Dynamic analysis of nanosize FG rectangular plates based on simple nonlocal quasi 3D HSDT", *Adv. Nano Res., Int. J.*, **7**(3), 191-208. https://doi.org/10.12989/anr.2019.7.3.191.

Chakraverty, S. and Pradhan, K.K. (2014), "Free vibration of functionally graded thin rectangular plates resting on Winkler elastic foundation with general boundary conditions using Rayleigh-Ritz method", *Int. J. Appl. Mech.*, **6**(4), 1450043.

Chen, C.S., Hsu, C.Y. and Tzou, G.J. (2009), "Vibration and stability of functionally graded plates based on a higher-order deformation theory", *J. Reinf. Plast. Comp.*, **28**(10), 1215-1234. https://doi.org/10.1177/0731684408088884.

Chikr, S.C., Kaci, A., Bousahla, A.A., Bourada, F., Tounsi, A., Bedia, E.A., Mahmoud, S.R. Benrahou, K.H. and Tounsi, A. (2020), "A novel four-unknown integral model for buckling response of FG sandwich plates resting on elastic foundations under various boundary conditions using Galerkin's approach", *Geomech. Eng., Int. J.*, **21**(5), 471-487. https://doi.org/10.12989/gae.2020.21.5.471.

Daikh, A.A. (2019), "Temperature dependent vibration analysis of functionally graded sandwich plates resting on Winkler/ Pasternak/Kerr foundation", *Mater. Res. Exp.*, **6**(6), 065702. https://doi.org/10.1088/2053-1591/ab097b.

Daikh, A.A. (2020), "Thermal buckling analysis of functionally graded sandwich cylindrical shells", *Adv. Aircr. Spacecr. Sci.*, **7**(4), 335-351. https://doi.org/10.12989/aas.2020.7.4.335.

Daikh, A.A. and Megueni, A. (2018), "Thermal buckling analysis of functionally graded sandwich plates", *J. Therm. Stress*, **41**(2), 139-159. https://doi.org/10.1080/01495739.2017.1393644.

Daikh, A.A., Houari, M.S.A. and Tounsi, A. (2019), "Buckling analysis of porous FGM sandwich nanoplates due to heat conduction via nonlocal strain gradient theory", *Eng. Res. Exp.*, **1**(1), 015022. https://doi.org/10.1088/2631-8695/ab38f9.

Daikh, A.A., Bensaid, I. and Zenmour, A.M. (2020a), "Temperature dependent thermomechanical bending response of functionally graded sandwich plates", *Eng. Res. Exp.*, **2**(1), 015006. https://doi.org/10.1088/2631-8695/ab638c.

Daikh, A.A., Drai, A., Bensaid, I., Houari, M.S.A. and Tounsi, A. (2020b), "On vibration of functionally graded sandwich nanoplates in the thermal environment", *J. Sandw. Struct. Mater.*, **2020**, 1099636220909790. https://doi.org/10.1177/1099636220909790.

Daikh, A.A., Guerroudj, M., El Adjrami, M. and Megueni, A. (2020c), "Thermal buckling of functionally graded sandwich beams", *Adv. Mater. Res.*, **1156**, 43-59. https://doi.org/10.4028/www.scientific.net/AMR.1156.43.

Dehshahri, K., Nejad, M.Z., Ziaee, S., Niknejad, A. and Hadi, A. (2020), "Free vibrations analysis of arbitrary three-dimensionally FGM nanoplates", *Adv. Nano Res., Int. J.*, **8**(2), 115-134. https://doi.org/10.12989/anr.2020.8.2.115.

Delale, F. and Erdogan, F. (1983), "The crack problem for a nonhomogeneous plane", *J. Appl. Mech.*, **50**, 609-614. https://doi.org/10.1115/1.3167098.

Dym, C.L. and Shames, I.H. (1973), *Solid Mechanics*, McGraw-Hill, New York, USA.

Ebrahimi, F. and Barati, M.R. (2017), "A third-order parabolic shear deformation beam theory for nonlocal vibration analysis of magneto-electro-elastic nanobeams embedded in two-parameter elastic foundation", *Adv. Nano Res., Int. J.*, **5**(4), 313-336. https://doi.org/10.12989/anr.2017.5.4.313.

Ehyaei, J. and Daman, M. (2017), "Free vibration analysis of double walled carbon nanotubes embedded in an elastic medium with initial imperfection", *Adv. Nano Res., Int. J.*, **5**(2), 179-192. https://doi.org/10.12989/anr.2017.5.2.179.

Ebrahimi, F. and Shafiei, N. (2017), "Influence of initial shear stress on the vibration behavior of single-layered graphene sheets embedded in an elastic medium based on Reddy's higher-order shear deformation plate theory", *Mech. Adv. Mater. Struct.*, **24,** 761-772. https://doi.org/10.1080/15376494.2016.1196781.

Ebrahimi, F. and Heidari, E. (2018), "Vibration characteristics of advanced nanoplates in humid-thermal environment incorporating surface elasticity effects via differential quadrature method", *Struct. Eng. Mech., Int. J.*, **68**(1), 131-157. https://doi.org/10.12989/sem.2018.68.1.131.

Ebrahimi, F. and Mahmoodi, F. (2018), "Vibration analysis of carbon nanotubes with multiple cracks in thermal environment", *Adv. Nano Res., Int. J.*, **6**(1), 57-80. https://doi.org/10.12989/anr.2018.6.1.057.

Ehyaei, J., Ebrahimi, F. and Salari, E. (2016), "Nonlocal vibration analysis of FG nano beams with different boundary conditions", *Adv. Nano Res., Int. J.*, **4**(2), 85-111. https://doi.org/10.12989/anr.2016.4.2.085.

Eringen, A.C. (1972), "Nonlocal polar elastic continua", *Int. J. Eng. Sci.*, **10**, 1-16. https://doi.org/10.1016/0020-7225(72)90070-5.

Eringen, A.C. (2002), *Nonlocal Continuum Field Theories*, Springer Science and Business Media, New York, USA.

Filonenko-Borodich, M.M. (1940), "Some approximate theories of elastic foundation", *Uchenyie Zapiski Moskovkogo Gosudarstuennogo Univ. Mekhanika*, **46**, 3-18.

George, N., Pitchaimani, J., Murigendrappa, S.M. and Lenin Babu,

M.C. (2018), "Vibro-acoustic behavior of functionally graded carbon nanotube reinforced polymer nanocomposite plates", *P. I. Mech. Eng. L. J. Mat.*, **232,** 566-581. https://doi.org/10.1177/1464420716640301.

Hetenyi, M. (1950), "A general solution for the bending of beams on an elastic foundation of arbitrary continuity", *J. Appl. Phys.*, **21**(1), 55-58. https://doi.org/10.1063/1.1699420.

Hołubowski, R., Glabisz, W. and Jarczewska, K. (2019), "Transverse vibration analysis of a single-walled carbon nanotube under a random load action", *Physica E Low Dimens. Syst. Nanostruct.*, **109**, 242-247. https://doi.org/10.1016/j.physe.2019.01.030.

Hosseini-Hashemi, S., Bedroud, M. and Nazemnezhad, R. (2013), "An exact analytical solution for free vibration of functionally graded circular/annular mindlin nanoplates via nonlocal elasticity", *Compos. Struct.*, **103,** 108-118. https://doi.org/10.1016/j.compstruct.2013.02.022.

Hussain, M., Naeem, M.N., Tounsi, A. and Taj, M. (2019), "Nonlocal effect on the vibration of armchair and zigzag SWCNTs with bending rigidity", *Adv. Nano Res., Int. J.*, **7**(6), 431-442. https://doi.org/10.12989/anr.2019.7.6.431.

Hussain, M., Naeem, M.N., Khan, M.S. and Tounsi, A. (2020a), "Computer-aided approach for modelling of FG cylindrical shell sandwich with ring supports", *Comput. Concrete, Int. J.*, **25**(5), 411-425. https://doi.org/10.12989/cac.2020.25.5.411.

Hussain, M., Naeem, M.N., Taj, M. and Tounsi, A. (2020b), "Simulating vibration of single-walled carbon nanotube using Rayleigh-Ritz's method", *Adv. Nano Res., Int. J.*, **8**(3), 215-228. https://doi.org/10.12989/anr.2020.8.3.215.

Kaddari, M., Kaci, A., Bousahla, A.A., Tounsi, A., Bourada, F., Tounsi, A., Bedia, E.A.A. and Al-Osta, M.A. (2020), "A study on the structural behaviour of functionally graded porous plates on elastic foundation using a new quasi-3D model: Bending and free vibration analysis", *Comput. Concrete, Int. J.*, **25**(1), 37-57. https://doi.org/10.12989/cac.2020.25.1.037.

Karami, B. and Karami, S. (2019), "Buckling analysis of nanoplate-type temperature-dependent heterogeneous materials", *Adv. Nano Res., Int. J.*, **7**(1), 51-61. https://doi.org/10.12989/anr.2019.7.1.051.

Karličić, D., Adhikari, S., Murmu, T. and Cajić, M. (2014), "Exact closed-form solution for nonlocal vibration and biaxial buckling of bonded multi-nanoplate system", *Compos. B Eng.*, **66**, 328-339. https://doi.org/10.1016/j.compositesb.2014.05.029.

Khiloun, M., Bousahla, A.A., Kaci, A., Bessaim, A., Tounsi, A. and Mahmoud, S.R. (2020), "Analytical modeling of bending and vibration of thick advanced composite plates using a four-variable quasi 3D HSDT", *Eng. Comput.*, **36**(3), 807-821.

Lee, C.Y. and Kim, J.H. (2013), "Hygrothermal postbuckling behavior of functionally graded plates". *Compos. Struct.*, **95**, 278-282. https://doi.org/10.1007/s00366-019-00732-1.

Lei, Z.X., Zhang, L.W. and Liew, K.M. (2016), "Analysis of laminated CNT reinforced functionally graded plates using the element-free kp-Ritz method", *Compos. B Eng.*, **84**, 211-221. https://doi.org/10.1016/j.compositesb.2015.08.081.

Malekzadeh, P. and Shojaee, M. (2015), "A two-variable first-order shear deformation theory coupled with surface and nonlocal effects for free vibration of nanoplates", *J. Vib. Control.*, **21**(14), 2755-2772. ttps://doi.org/10.1177/1077546313516667.

Matouk, H., Bousahla, A.A., Heireche, H., Bourada, F., Bedia, E. A., Tounsi, A., Mahmoud, S.R., Tounsi, A. and Benrahou, K.H. (2020), "Investigation on hygro-thermal vibration of P-FG and symmetric S-FG nanobeam using integral Timoshenko beam theory", *Adv. Nano Res., Int. J.*, **8**(4), 293-305. https://doi.org/10.12989/anr.2020.8.4.293.

Pasternak, P.L. (1954), "Fundamentals of a new method of analyzing structures on an elastic foundation by means of two foundation moduli", *Proceedings of the Gosudarstvennoe Izdatelstro Liberaturi po Stroitelstvui Arkhitekture*, Moscow, Russia.

Rahmani, M.C., Kaci, A., Bousahla, A.A., Bourada, F., Tounsi, A., Bedia, E.A., Mahmoud, S.R., Benrahou, K.H. and Tounsi, A. (2020), "Influence of boundary conditions on the bending and free vibration behavior of FGM sandwich plates using a four-unknown refined integral plate theory", *Comput. Concrete, Int. J.*, **25**(3), 225-244. https://doi.org/10.12989/cac.2020.25.3.225.

Semmah, A., Heireche, H., Bousahla, A.A. and Tounsi, A. (2019), "Thermal buckling analysis of SWBNNT on Winkler foundation by non local FSDT", *Adv. Nano Res., Int. J.*, **7**(2), 89-98. http://dx.doi.org/10.12989/anr.2019.7.2.089.

Shariati, A., Ghabussi, A., Habibi, M., Safarpour, H., Safarpour, M., Tounsi, A. and Safa, M. (2020), "Extremely large oscillation and nonlinear frequency of a multi-scale hybrid disk resting on nonlinear elastic foundation", *Thin-Wall. Struct.*, **154,** 106840. https://doi.org/10.1016/j.tws.2020.106840.

Singh, S.J. and Harsha, S.P. (2020), "Thermo-mechanical analysis of porous sandwich S-FGM plate for different boundary conditions using Galerkin Vlasov's method: A semi-analytical approach", *Thin-Wall. Struct.*, **150**, 106668. https://doi.org/10.1016/j.tws.2020.106668.

Singh, S.J. and Harsha, S.P. (2019), "Nonlinear dynamic analysis of sandwich S-FGM plate resting on pasternak foundation under thermal environment", *Eur. J. Mech. A Solids*, **76**, 155-179. https://doi.org/10.1016/j.euromechsol.2019.04.005.

Taj, M., Majeed, A., Hussain, M., Naeem, M.N., Safeer, M., Ahmad, M., Khan, H.U. and Tounsi, A. (2020), "Nonlocal orthotropic elastic shell model for vibration analysis of protein microtubules", *Comput. Concrete, Int. J.*, **25**(3), 245-253. https://doi.org/10.12989/cac.2020.25.3.245.

Tounsi, A., Al-Dulaijan, S.U., Al-Osta, M.A., Chikh, A., Al-Zahrani, M.M., Sharif, A. and Tounsi, A. (2020), "A four variable trigonometric integral plate theory for hygro-thermo-mechanical bending analysis of AFG ceramic-metal plates resting on a two-parameter elastic foundation", *Steel Compos. Struct.*, **34** (4), 511-524. http://dx.doi.org/10.12989/scs.2020.34.4.511.

Winkler, E. (1867), *Theory of Elasticity and Strength*, Dominicus Prague, Czechoslovakia.

Yang, J. and Shen, H.S. (2002), "Vibration characteristics and transient response of shear-deformable functionally graded plates in thermal environments", *J. Sound Vib.*, **255**(3), 579-602. https://doi.org/10.1006/jsvi.2001.4161.

Zine, A., Bousahla, A.A., Bourada, F., Benrahou, K.H., Tounsi, A., Adda Bedia, E.A., Mahmoud, S.R. and Tounsi, A. (2020), "Bending analysis of functionally graded porous plates via a refined shear deformation theory", *Comput. Concrete, Int. J.*, **26**(1), 63-74. https://doi.org/10.12989/cac.2020.26.1.063.

CC